R-05-71

Preliminary assessment of potential underground stability (wedge and spalling) at Forsmark, Simpevarp and Laxemar sites

Derek Martin, University of Alberta

December 2005

Svensk Kärnbränslehantering AB
Swedish Nuclear Fuel
and Waste Management Co
Box 5864
SE-102 40 Stockholm Sweden
Tel 08-459 84 00
+46 8 459 84 00
Fax 08-661 57 19
+46 8 661 57 19

ISSN 1402-3091
SKB Rapport R-05-71

Preliminary assessment of potential underground stability (wedge and spalling) at Forsmark, Simpevarp and Laxemar sites

Derek Martin, University of Alberta

December 2005

Summary

In SKB's Underground Design Premises /SKB 2004/ the objective in the early design phase is to estimate if there is sufficient space for the repository at a site. One of the conditions that could limit the space available is stability of the underground openings, i.e., deposition tunnels and deposition boreholes. The purpose of this report is to provide a preliminary assessment of the potential for wedge instability and spalling that may be encountered at the Forsmark, Simpevarp and Laxemar sites based on information from the site investigations program up to July 30, 2004.

The rock mass spalling strength was defined using the in-situ results from SKB's Äspö Pillar Stability Experiment and AECL's Mine-by Experiment. These experiments suggest that the rock mass spalling strength for crystalline rocks can be estimated as 0.57 of the mean laboratory uniaxial compressive strength. A probability-based methodology utilizing this in-situ rock mass spalling strength has been developed for assessing the risk for spalling in a repository at the Forsmark, Simpevarp and Laxemar sites. The in-situ stresses and the uniaxial compressive strength data from these sites were used as the bases for the analyses.

Preliminary findings from all sites suggest that, generally, the risk for spalling increases as the depth of the repository increases, simply because the stress magnitudes increase with depth. The depth at which the risk for spalling is significant, depends on the individual sites which are discussed below.

The greatest uncertainty in the spalling analyses for Forsmark is related to the uncertainty in the horizontal stress magnitudes and associated stress gradients with depth. The confidence in these analyses can only be increased by increasing the confidence in the stress and geology model for the site. From the analyses completed it appears that spalling in the deposition tunnels can be controlled by orienting the tunnels approximately parallel to the maximum horizontal stress. The analyses indicates however that the risk of spalling for the deposition holes increases below a depth 550 m.

The spalling analyses for Simepvarp and Laxemar suggest that spalling will not be an issue in the deposition tunnels or deposition holes down to a depth of 650 m for Stress Domain II. In Stress Domain I, the analyses indicates that the risk for spalling in the deposition holes increases significantly below a depth of 450 m. It should be noted the experience with the underground excavations at a depth of 450 m at the nearby Äspö Hard Rock Laboratory which is in a similar rock mass to that found at Simpevarp and Laxemar and similar stress domain as Domain I, did not show any evidence of spalling. The mean laboratory uniaxial compressive strength for the Simepvarp and Laxemar sites, which is used to estimate the rock mass spalling strength, is considerably less than that used for the Äspö diorite and hence may be under estimated. This needs further investigations.

The results from the Äspö Pillar Stability Experiment that utilized 1.8-m-diameter boreholes suggest that should spalling be severe, as in this experiment, the increased borehole volume due to spalling could approach 0.18 m^3. This volume increase is approximately 18% greater then the 0.150 m^3 proposed in /SKB 2004/ as an acceptable volume increase per deposition hole. In the Äspö Pillar Stability Experiment the spalling was caused by excavation-induced stresses, i.e., after drilling, and thermally-induced

stresses. The volume of spalling after drilling was approximately 30% of the total spalling volume. Hence it is highly unlikely that the volume increase caused by drilling-induced spalling will exceed the proposed allowable volume increase for any site.

Wedge analysis requires detailed knowledge of the fracture system at the repository level. It was concluded that the DFN model may not contain sufficient information at this time for detailed wedge stability analyses and hence may not be appropriate at this stage of site investigation. Nonetheless a preliminary wedge analysis for Forsmark was carried out to demonstrate the methodology that could be employed using the Discrete Fracture Network (DFN) model. These analyses showed that the risk for wedge instability was very minor and that these wedges could be handled by normal Scandinavian tunnel support practice. These results are in keeping with construction experience from SKB underground facilities at Forsmark (SFR), Clab and Äspö HRL suggests that wedge stability is not likely to significantly influence the layout of repository or the preliminary design of the repository.

Sammanfattning

I SKB:s rapport Underground dEsign Premises /SKB, 2004/ är ett av målen med den inledande projekteringen att bedöma om platsen är tillräckligt stor för ett slutförvar. En av de faktorer som kan påverka tillgänglig plats är stabiliteten för undermarksutrymmena, främst deponeringstunnlar och -hål. Syftet med denna rapport är att göra en preliminär bedömning av risken för instabilitet på grund av kilar och spänningsinducerade spjälkbrott vid Forsmark, Simpevarp och Laxemar, baserad på resultat som fanns tillgängliga upp till och med juli 2004.

Bergmassans hållfasthet mot spänningsinducerat spjälkbrott har definierats utifrån de fullskaliga försöken av SKB - Äspö Pillar stability Experiement (APSE) och AECLs Mine-by Experiment. Resultaten från dessa båda försök visar att bergmassans hållfasthet mot spänningsinducerat spjälkbrott kan bestämmas till 0,57 av medelvärdet från enaxliella tryckförsök. En sannolikhetsbaserad ansats har gjorts för att värdera risken för spänningsinducerat spjälkbrott i ett slutförvar beläget i Forsmark, Simpevarp eller Laxemar.

Preliminära resultat från analysen av samtliga platser visar generellt att risken för spänningsinducerat spjälkbrott ökar med djupet, eftersom spänningsmagnituder ökar med djupet. Det djup där risken för spänningsinducerat spjälkbrott kan vara signifikant varierar mellan platserna, se nedan. I samtliga studerade fall kan risken för spänningsinducerat spjälkbrott i deponeringstunnlarna minska radikalt, eller elimineras helt genom att orientera dessa parallellt med största horisontalspänningen.

Den största osäkerheten i resultaten av spänningsinducerat spjälkbrott i Forsmark beror på osäkerheten i magnitud för de horisontella spänningarna, samt dess gradient mot djupet. Konfidensen i dessa analyser kan förbättras främst genom att öka tilltron till platsens spännings- och geologimodeller. Enligt utförda analyser kan risken för spänningsinducerat spjälkbrott kontrolleras om tunnlarna orienteras ungefär parallellt med den största horisontalspänningen. Det finns dock en ökande risk för spjälkbrott i deponeringshål under ca 550 m djup.

Analyser av spänningsinducerat spjälkbrott för Simpevarp och Laxemar indikerar att spänningsinducerat spjälkbrott inte är ett problem inom spänningsdomän II åtminstone ner till 650 m djup. Inom spänningsdomän I pekar analyserna på risk för spänningsinducerat spjälkbrott i deponeringshål under ett djup av ca 450 m. Dock bör noteras, att erfarenheterna från undermarksarbeten i det närliggande Äspö Hard Rock Laboratory på samma djup i liknande berg, och med liknande spänningar som i domän I inte visar några tecken på spänningsinducerade spjälkbrott. Medelvärdet för den enaxliga tryckhållfastheten ifrån Simpevarp och Laxemar, som använts i denna rapport för analys av risken för spänningsinducerat spjälkbrott, är signifikant lägre än motsvarande resultat från Äspö dioriten, och kan därmed vara underskattad. Detta behöver utredas närmare.

Resultaten från APSE, som genomfördes i fullskaliga deponeringshål med diameter 1,8 m, indikerar att en omfattande spjälkbrott kan orsaka ett utfall av storleksordninge 0,18 m3 för ett deponeringshål. Detta är ca 18 % större än de 0,15 m3 som föreslogs i /SKB, 2004/ som den acceptabla volym överberg för ett deponeringshål. I APSE orsakades spjälkbrottet av både själva borrningen och av termo-inducerade spänningar. Utfallande

volym i samband med borrningen var ca 30 % av den totalt avspjälkade volymen. I jämförelse med de studerade platserna är det inte troligt att spänningsinducerat spjälkbrott i samband med borrning av deponeringshål på någon av de studerade platserna skulle orsaka utfall av överberg över de ansatta måtten.

Analys av risken för kilutfall kräver kunskaper om sprickfördelningen på förvarsdjupet. Det bedöms att befintliga DFN-modeller troligen inte ännu innehåller tillräckligt detaljerad information för kilbrottsanalyser, och kan därför vara olämpliga för detta syfte i det relativt tidiga projekteringsskedet som denna studie gjorts för. En preliminär kilbrottsanalys genomfördesändå för Forsmark med stöd av platsbeskrivningens DFN-modell. Analysen visade på mycket liten risk för instabila kilar, och att dessa risker borde kunna hanteras med sedvanlig skandinavisk praxis för bergförstärkning. Erfarenheter från SKB:s undermarksanläggningar i Forsmark (SFR), Clab and Äspö HRL indikerar dessutom att kilstabilitet troligen inte är en fråga som har signifikant påverkan på layout eller preliminär design för slutförvaret.

Contents

1 Introduction

In SKB's Underground Design Premises /SKB 2004/ the objective in the early design phase is to estimate if there is sufficient space for the repository at a site. One of the conditions that could limit the space available is stability of the underground openings, i.e., deposition tunnels and deposition boreholes. Stability issues likely to be encountered at a repository are discussed in detail in Martin et al. /2001/. The two major stability issues considered in this report that could impact the design of the repository are (see Figure 1–1):

1. Structurally controlled gravity driven instability, referred to wedges or falls-of-ground
2. Stress-driven instability referred to as spalling or slabbing.

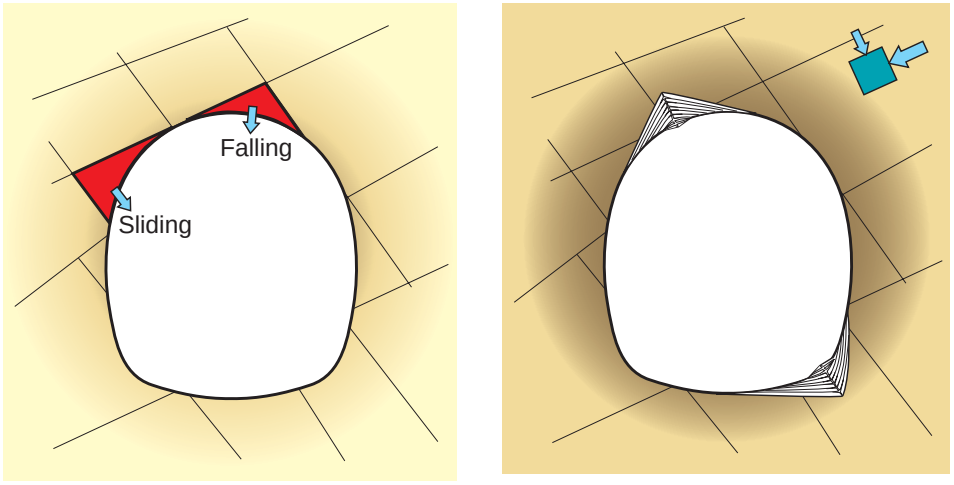

(a) Wedge failure ***(b)*** Spalling failure

Figure 1–1: *Illustration of the two significant modes of underground instability anticipated at a repository.*

The purpose of this report is to provide a preliminary assessment of the potential for wedge instability and spalling that may be encountered at the Forsmark and Oskarshamn sites[1] at the depths of a repository (400, 500, 600 and 700 m) based on information from the site investigations program up to July 30, 2004. The issues to be addressed in this report are:

1. The orientation of deposition tunnels that would minimise the volume of unstable wedges in deposition tunnels.
2. The orientation of deposition tunnels with a view towards minimising the risk of spalling.
3. The loss of deposition holes due to the risk of spalling.

[1]Oskarshamn covers both the Simpevarp peninsula and Laxemar (the main inland) sites

At this stage in the site investigations and preliminary design it is not possible to answer the questions above explicitly. Therefore, a probabilistic approach will be employed that utilizes the range of data that are currently available.

2 Risk terminology

Geotechnical engineering is fundamentally about managing risk. Morgenstern /1995/ summarized risk assessment concepts using the framework for risk management adopted by the Canadian Standards Association (Figure 2–1). Figure 2–1 is a generalised framework for risk management that would need to be modified for individual projects. But in all cases risk assessment requires identification of the hazard and quantifying the risk associated with each hazard. Morgenstern noted that while quantitative risk analysis (QRA) is one aspect of the framework, qualitative risk assessment is also a valuable component of risk management. With risk defined as the combination of the probability of occurrence of an undesired event and the possible extent of the event's consequence, risk can, in principle, be calculated. The full potential of QRA is best met with the establishment of acceptable risk criteria. Establishing acceptable risk criteria in geotechnical engineering is a challenge that is evolving. Relating consequences to cost/benefit analysis provides a simpler basis for evaluating acceptable risk. The link between risk and benefit must be balanced and within the context of geotechnical engineering the risks are usually reduced to an acceptable standard by the best practical means. This report is written within this context.

Swedish regulations state that probability based methods, such as the partial coefficient method, should be used in geotechnical design. However, Stille et al. /2003/ suggest that this approach is too restrictive and probability based methods should be used throughout the whole design and construction process. In their report they use the following definitions:

Hazard: a source of a potential damage event.

Damage event: an event that may cause damage to humans, properties or the environment.

Risk: the combined effect of the probability of a damage event and the consequences caused by the damage event.

In the following section a risk based methodology is proposed that follows the general principles suggested by Stille et al. /2003/ for assessing risk in rock engineering. Firstly

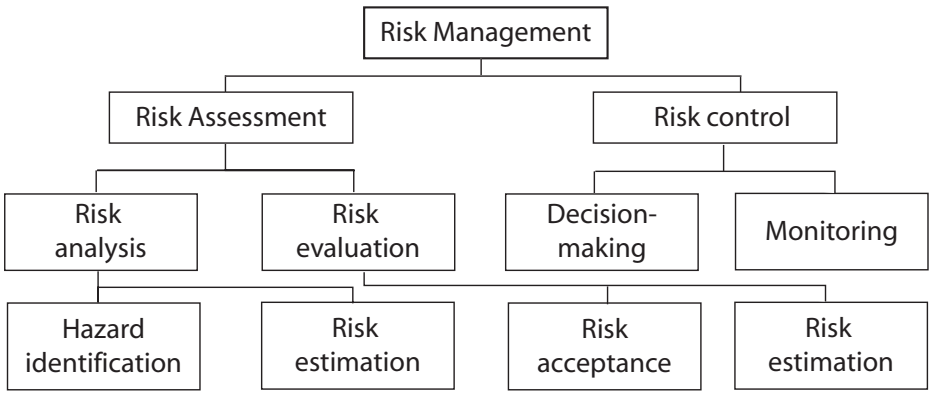

Figure 2–1: *A general framework for risk management proposed by the Canadian Standards Association Canadian Standard Association /1991/.*

the hazards identified in Figure 1–1 are evaluated as potential damage events and the severity of the hazard assessed by its magnitude, e.g., size of the wedge or depth of spalling failure. The risk can only be assessed after these two steps are completed and is beyond the scope of this report.

3 Risk based methodology

A general methodology that can be used to assess the wedge and spalling hazard is illustrated in Figure 3–1. The methodology in this report is restricted to that noted above the 'risk control options' in Figure 3–1. For each hazard a criterion is required that can be used to determine the frequency of occurrence. Once the frequency of the hazard has been determined the next step is to assess the severity of the hazard. The approach for each hazard is discussed in the following sections.

3.1 Wedge stability methodology

In this section the software program UnWedge was used for all the wedge related calculations. UnWedge[2] is a Windows based program that incorporates limit equilibrium with in-situ stress to evaluate the stability of wedges around underground openings. Other software programs may be equally suitable for this task.

3.1.1 Frequency of Wedges

When continuous fractures from three joint sets are intersected by an underground opening a tetrahedral wedge can form. These three joints and the underground surface provide the kinematic freedom for a wedge to slide or fall under the influence of gravity (see Figure 3–2a). In Figure 3–2a the wedge is located in the centre of a 5-m diameter tunnel and will simply fall under the weight of gravity and hence have the factor of safety of zero. For this example, in-situ stress was ignored in the calculation; however, if the effect of in-situ stress is included in the calculation the factor of safety for the roof wedge in Figure 3–2a increases from zero to approximately 38. This improvement in the factor of safety arises because the in-situ stresses increase the normal stress (confinement) acting on the failure planes Martin et al. /2001/. Hence, in-situ stress can play a significant role in the stability of underground wedges, and should be considered in the assessing the frequency of occurrence, and the severity of the hazard, i.e., the size of the wedge.

3.1.2 Severity of Wedges

Once a wedge forms the next step was to evaluate the severity of the hazard, which is a function of the size of the opening. In this case the severity was quantified by estimating the size and weight of the wedge which are automatically calculated by UnWedge.

3.1.3 Wedge data uncertainty and probability

At this stage in the design the main objective is to assess if wedges are likely to be of concern for detailed design or construction. For these analyses the shear strength of all joints is assumed to have a constant friction angle with zero cohesion. This approach will show the relationship of joint orientation and tunnel orientation on the formation of wedges.

[2] Available from WWW.RocScience.com

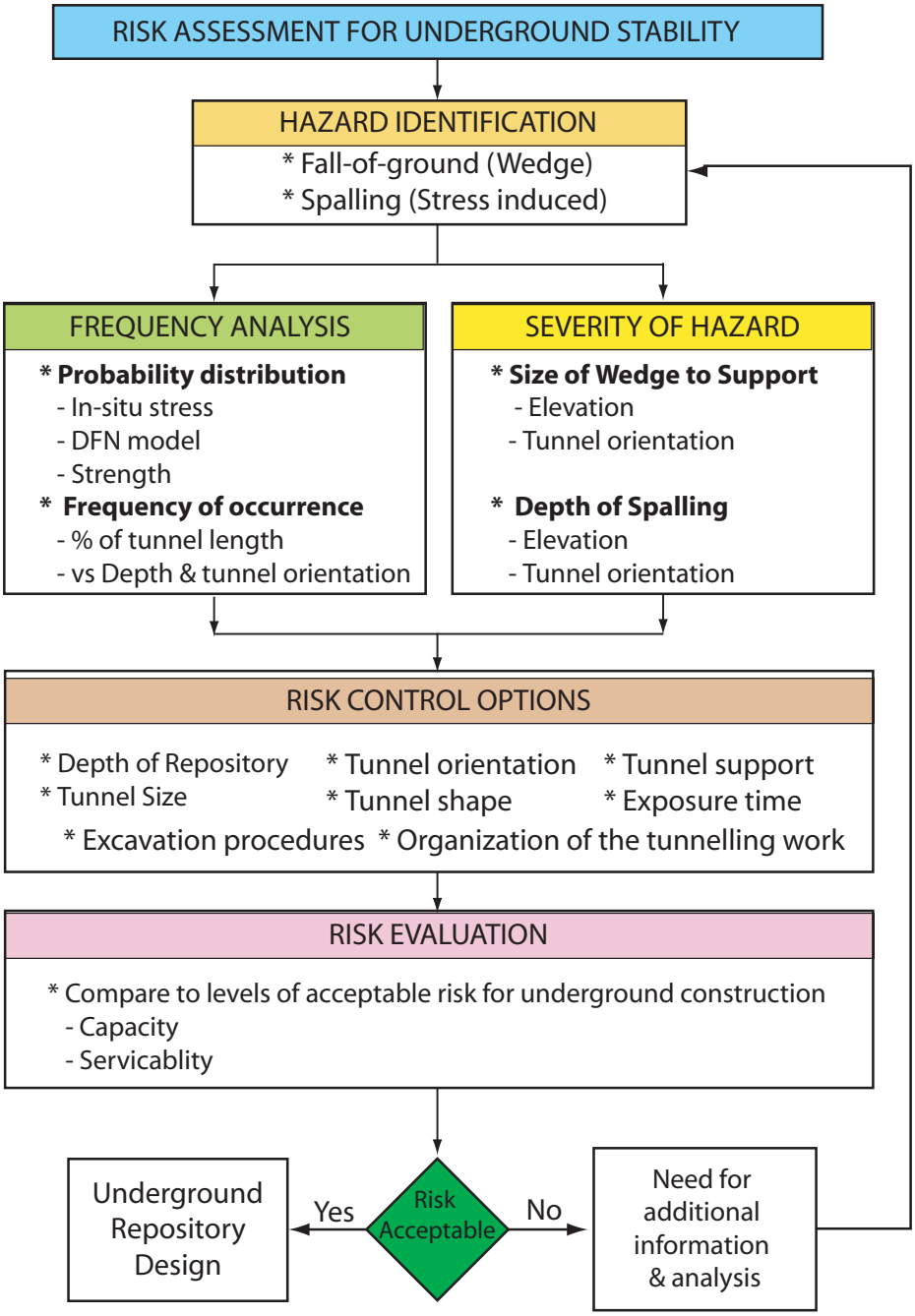

Figure 3–1: *Illustration of the steps involved in assessing the risk for wedge instability and spalling. This report is focused on developing the methodology for assessing the severity of the hazard and does not address "risk evaluation"*

The major assumption is that the three joints required to form the wedge are present and that the joint surfaces are sufficiently large to form the wedge. The probability that this will occur resides with the development of the Discrete Fracture Network (DFN) model used to establish the joint orientations. Hence, the orientation of the joints is held constant over the depths investigated, unless the DFN has a depth dependency.

As indicated in Martin et al. /2001/ tunnel intersections can lead to wedge stability issues. This special case has not been addressed in this report.

Table 3–1: The following input parameters were used for the wedge analyses in this report. The input values for the fractures were obtained from the Discrete Fracture Network Model (DFN).

	Input parameter	Values used in analysis
1.	Number of joint sets, orientations and trace length	Based on DFN model. Independent of depth
2.	Joint strength	ϕ_j = constant, Cohesion=0
3.	In-situ stress	Mean magnitude and orientation of the principal stresses at each depth of interest. Values vary with depth.
4.	Deposition Tunnel: 5-m-diameter	Trend varies from 0 to 360 degrees in 30 degree intervals. Plunge=0
5.	Deposition Borehole: 1.8-m-diameter	
	Vertical	Plunge = Vertical (90 degrees)
	Horizontal	Trend varies from 0 to 360 degrees in 30 degree intervals

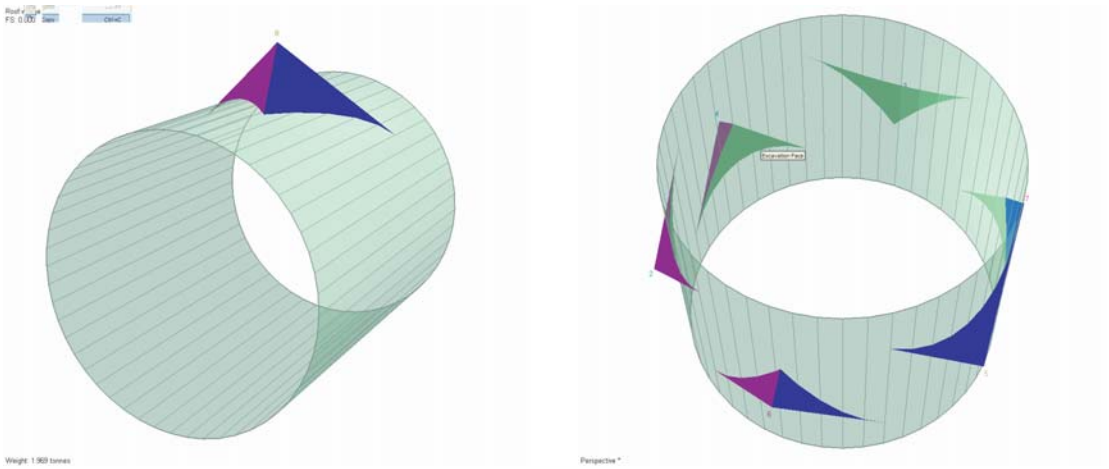

(a) Deposition tunnel ***(b)*** Deposition borehole

Figure 3–2: *Example of a wedge located in the roof of a deposition tunnel (left figure) and the wedges formed in a vertical shaft (right figure) using the RocScience Software UnWedge. In the right figure all the wedges are stable while in the left figure the wedge will fall from the roof if the effect of in-situ stress is ignored.*

3.2 Spalling assessment methodology

When the stresses on the boundary of an underground excavation reach the rock mass strength failure occurs. In good quality hard rock, such as that found in the Scandinavian Shield, the failure process is described as "spalling" and the associated rock mass strength as the "spalling strength". The word spalling is purposely used to indicate that the failure process involves extensional splitting/cracking and is a different failure process from that of shearing which is commonly observed in weak rocks. Appendix A.2 provides an overview and the background to the rock mass spalling strength that is used in this report.

Spalling is generally defined as the formation of stress-induced slabs on the boundary of an underground excavation (see Figure 3–3a). It initiates in the region of maximum tangential stresses and results in a v-shaped notch that is local to the boundary of the opening (see Figure 3–3b) . The slabs can vary in thickness from a few millimeters to a few centimeters, for circular underground openings that range in diameter from 1 to 5 m. A detailed review of the spalling process was provided by Martin et al. /2001/.

In order to determine if spalling will occur the rock mass spalling strength must be established. Since 1990 two major experiments have been carried out to develop a methodology for assessing the rock mass spalling strength for crystalline rocks: (1) AECL's Mine-by Experiment Martin and Read /1996/, and (2) Äspö Pillar Stability Experiment (APSE) Andersson /2005/. The rock mass spalling strength used in this report, i.e., the tangential stress required to initiate spalling on the boundary of an opening in crystalline rock, is based on the findings from these experiments (see Appendix A.2 for a brief summary of those experiments). Based on the findings from those experiments the rock mass spalling strength (σ_{sm}), given in Table 3–2, was used for the analyses in this report.

In Table 3–2 the rock mass spalling strength (σ_{sm}) is normalized to the mean laboratory uniaxial compressive strength[3]. This ratio provides a method for evaluating the rock mass spalling strength for other sites when only the laboratory uniaxial compressive strength is known. Note that the mean laboratory uniaxial compressive strength is used and not the range in measured laboratory uniaxial compressive strength.

Because of the variability of the rock mass at some sites, the rock mass spalling strength in Table 3–2 may need to be checked periodically. The onset of extension cracking (dilation) in laboratory uniaxial samples can be used to indicate the boundary for the initiation of damage in brittle rock (see Appendix A for a more complete discussion). Crack initiation

[3]The mean uniaxial strength, rather then the full range of uniaxial strength, was found to provide better agreement with field observations.

Table 3–2: The rock mass spalling strength used in this report.

	σ_{sm} (MPa)	$\sigma_{sm}/UCSm$
Coarse & medium grained crystalline rocks	120 ± 5	0.57 ± 0.02

UCSm= Mean laboratory uniaxial compressive strength
σ_{sm} = Rock mass spalling strength
$\pm$ = Minimum, maximum

(a) Spalling slabs

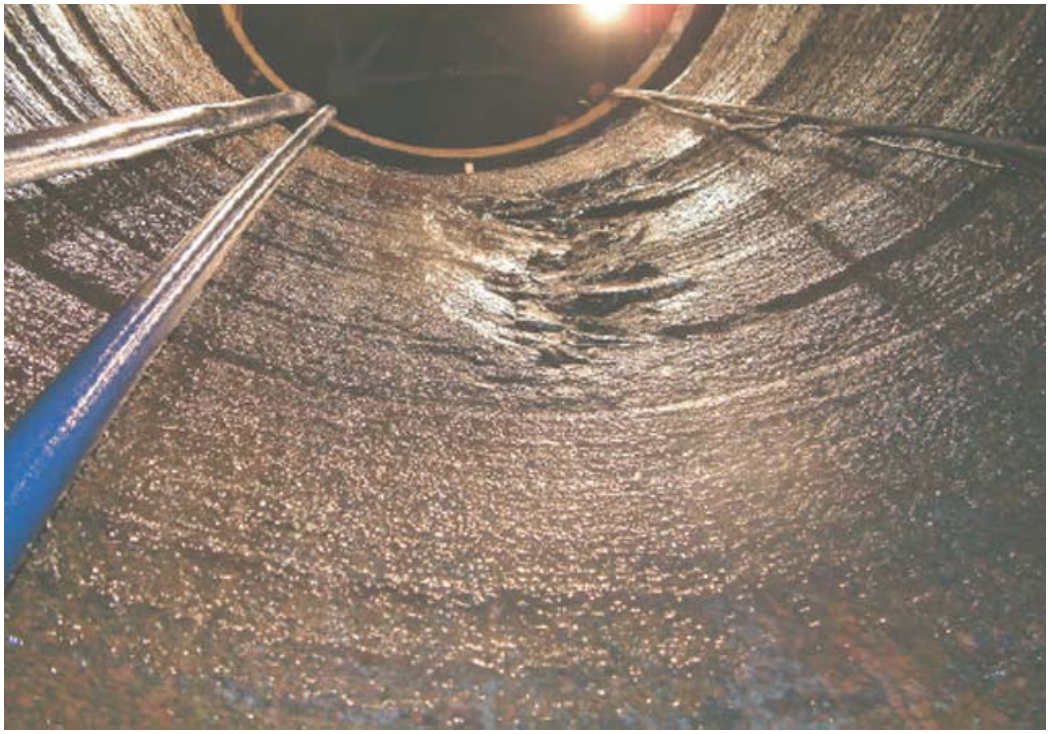

(b) V-shaped notch

Figure 3–3: *Examples of spalling observed around a 1.8-m-diameter borehole in the ÄPSÖ Pillar Stability Experiment Andersson /2005/. Photos provided by C. Andersson.*

in laboratory uniaxial tests represents a lower bound limit for the spalling rock mass strength and may occur between 0.4 and 0.6 of the mean uniaxial compressive strength.

3.2.1 Spalling criterion

The potential for spalling is assessed using a traditional factor of safety approach that compares Demand to Capacity. If the magnitude of the maximum tangential elastic stresses ($\sigma_{\theta\theta}$) on the boundary of an underground opening (Demand) reaches the rock mass spalling strength (Capacity) the factor of safety can be expressed as:

$$\text{Factor of Safety} = \frac{\sigma_{sm}}{\sigma_{\theta\theta}} \tag{1}$$

The maximum tangential elastic stress on the boundary of circular opening in a continuous, homogeneous, isotropic and linearly elastic rock can be expressed using the well known Kirsch equations for plane strain:

$$\sigma_{\theta\theta} = 3\sigma_{\max} - \sigma_{\min} \tag{2}$$

where $\sigma_{\max}$ and $\sigma_{\min}$ are the maximum and minimum far-field principal stresses, respectively, in the plane of analysis.

In the criterion above, determining the maximum tangential stress is essential for evaluating the potential for spalling. It should be noted that the maximum tangential stress is a function of the tunnel profile shape and the orientation of the tunnel relative to the in-situ stress tensor. Numerical analyses are required to determine the maximum tangential stress on the boundary of non-circular tunnels, e.g., horse-shoe shaped tunnels.

3.2.2 Severity of Spalling

Depth of spalling

Once the stresses on the boundary of the excavation reach the rock mass spalling strength (Factor of safety for spalling ≤ 1) and spalling initiates, the severity of the hazard must be assessed, i.e., how deep will the spalling extend. The depth of spalling can be estimated using the empirical correlations described in Martin et al. /2001/ and given in Figure 3–4. These data were compiled from published case histories in a wide range of rock mass conditions and in-situ stresses. The results from the Äspö Pillar Stability Experiment (APSE) have been added to Figure 3–4 and Figure 3–4 shows that the empirical correlations predicted the depth of spalling for the Äspö Pillar Stability Experiment reasonably well.

In Figure 3–4 the depth of spalling is normalized to the tunnel radius and is measured from the centre of the tunnel. The expression for the depth of spalling given in Figure 3–4 for approximately circular openings can be rewritten as:

$$S_d = a\left(0.5\frac{\sigma_{\theta\theta}}{\sigma_{sm}} - 0.52\right) \text{ for } \sigma_{\theta\theta} > \sigma_{sm} \tag{3}$$

where the S_d is measured from the boundary of the tunnel (see Figure 3–5).

Andersson /2005/ observed that the depth of spalling in the Äpsö Pillar Stability experiment was influenced locally by existing fractures. However, as shown by Figure 3–4 it is not anticipated that existence of fractures will significantly affect the average depth of spalling calculated using Equation 3.

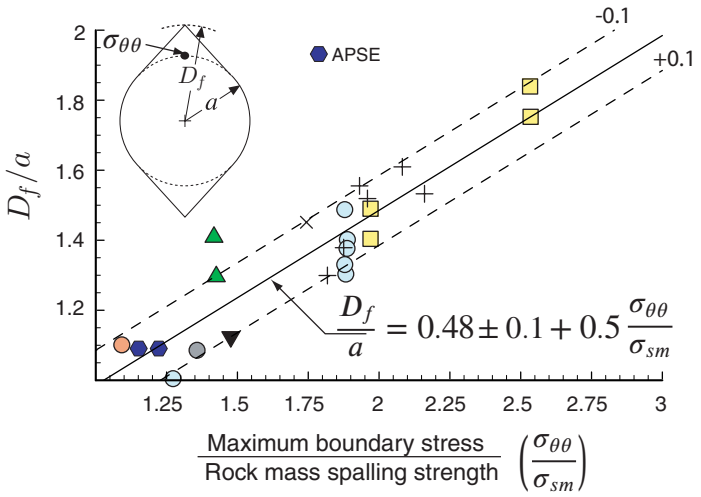

Figure 3–4: *Empirical relationship used to establish the severity of the hazard, i.e., the depth of spalling. Data from Martin et al. /2001/. Also shown are the new data from the Äpsö Pillar Stability experiment (APSE) Andersson /2005/.*

Volume of spalling

The volume of spalling in a deposition can be estimated using the data from the Äspö Pillar Stability Experiment. In this experiment the slabs of rock were carefully removed to expose the shape of the notch.. It is assumed that these slabs would also be removed at a repository during the excavation process. Measurements of the extent of spalling after the drilling and heating of the 1.8-m-diameter borehole showed that the spalling starts at some depth below the tunnel floor and does not extend to the bottom of the borehole Andersson /2005/ (see Figure 3–5). Similar findings were observed at AECL's URL suggesting that an Excavation Disturbed Zone will exist around all underground openings at the repository depth that reduces the tangential stress concentrations near the boundary of the tunnel. Based on the experience from AECL's Mine by Experiment, this effect is more pronounced in drill-and-blast tunnels than machine excavated tunnels. In addition, the spalling does not extend to the bottom of the borehole because of the reduced tangential stresses at the bottom of the borehole caused by the three dimensional stress effect. Using this data it would appear that a reasonable approximation for the vertical extent of spalling in deposition holes can be estimated by taking 75% of the total length of the deposition hole.

Figure 3–6 illustrates the spalling area observed on one side of a deposition hole and sequence of calculations required to determine the area of spalling. The area of spalling as illustrated in Figure 3–6 can be determined using the equations associated with the sector and segment of a circle and the area of triangle.

Using the definitions in Figure 3–6, Area 1 can be determined by:

$$\begin{aligned} A_1 &= 1/2 l(S_d + z) \\ &= 1/2(R\sin\theta/2)(S_d + (R - R\cos\theta/2)) \end{aligned}$$

where S_d is the depth of spalling predicted by Equation 3 and θ is given in radians. Note that the angle θ is given by $2\arcsin(l/2R)$.

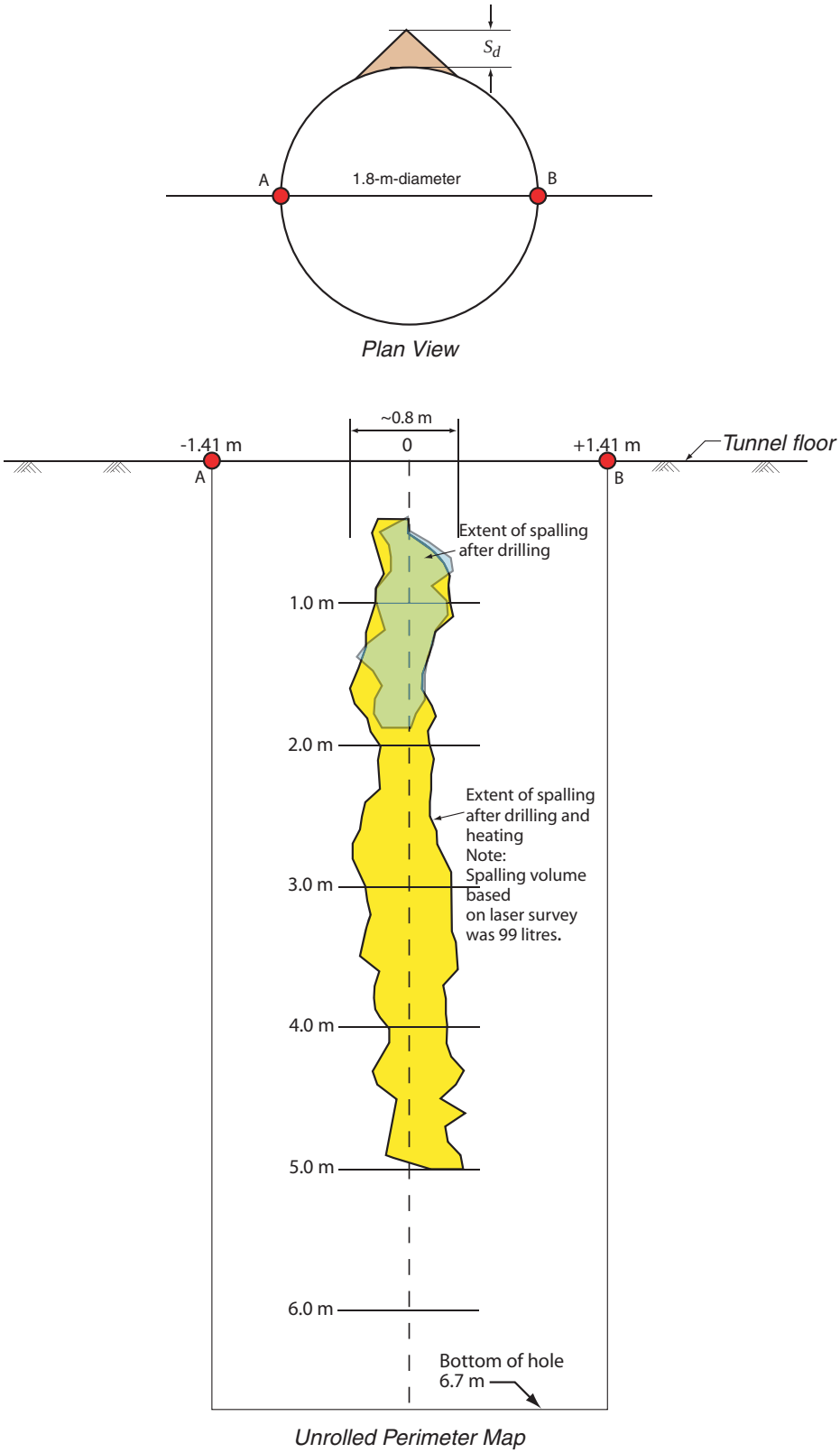

Figure 3–5: *Extent of spalling observed in the Äspö Pillar Stability Experiment. Data provided by C. Anderson (SKB).*

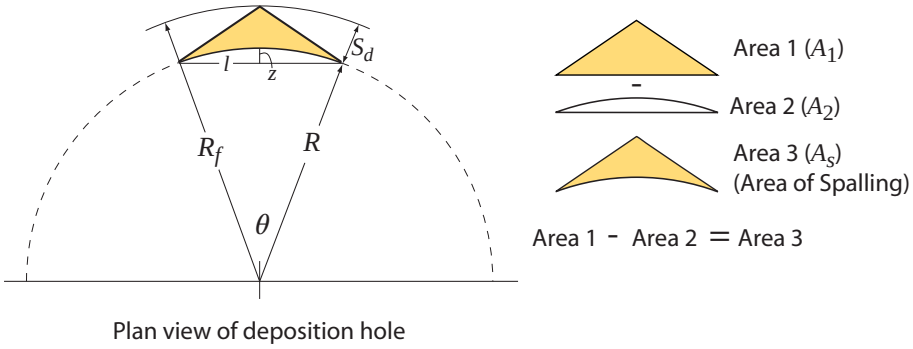

Figure 3–6: *Illustration of the spalling area and labelling used in deriving Equation 4.*

And, Area 2 is given by:

$$A_2 = 1/2R^2(\theta - \sin\theta)$$

The area of spalling (A_s) is then given by:

$$\begin{aligned} A_s &= A_1 - A_2 \\ &= 1/2(R\sin\theta/2)(S_d + (R - R\cos\theta/2)) - 1/2R^2(\theta - \sin\theta) \end{aligned}$$

Simplifying

$$A_s = \frac{1}{2}R\left(2(R + S_d)\sin\frac{\theta}{2} - R\theta\right) \tag{4}$$

The lateral extent of spalling (l in Figure 3–6) based on the data from Äspö Pillar Stability Experiment was approximately 0.8 m. This would give $\theta = 53$ degree. Using $R = 0.9$m, $\theta = 0.921$, and $S_d = 0.07$m, the area of spalling for the APSE borehole given by Equation 4 is approximately 0.016m^2. Combining the area of spalling, with the vertical extent after drilling (1.5 m) and heating (75% of 6.7 m) the volume of spalling (S_v) for the APSE borehole would be approximately 0.023m^3 after drilling and 0.08m^3 after drilling and heating. The volume of spalling for the APSE borehole after drilling and heating measured using laser scanning was 0.089m^3. Hence if the stress magnitudes created for the Äspö Pillar Stability Experiment existed at the repository level the total volume of spalling after drilling would be 0.046m^3 and 0.160m^3 after drilling and heating assuming the hole remained open. This total spalling volume of 0.160m^3 is approximately equal to the 0.150m^3 specified in SKB /2004/ as being an acceptable volume increase per deposition hole. Hence it is unlikely that volume increase due to spalling of the deposition holes will exceed the allowable volume increase. Nonetheless the approach described above can be used estimate the volume loss due to spalling once the probability of spalling is encountered.

The angle θ of 53 degree in Figure 3–6 for the APSE 1.8-m-diameter borehole is similar to the angles reported at AECL's Underground Research Laboratory. For example, the spalling that formed during the diamond drilling of a 1.25-m diameter, 5-m-deep, borehole gave $\theta \approx 45$ degree, while θ of approximately 65 degree was measured for the 3.5-m diameter Mine-by tunnel. Brudy et al. /1995/ showed that for the deep KTB borehole θ remained relatively constant at about 30 to 55 degree from a depth of 3000 m to a depth of

5500 m. Barton et al. /1988/ reported similar findings from the Fenton geothermal site where θ averaged 76 degree between a borehole depth of 2829 and 3627 m. Hence, $\theta = 53$ degree for the APSE 1.8-m-diameter borehole is in keeping with existing experience and may be used to calculate the spalling volume for deposition hopes.

It should be noted that by using a constant $\theta = 53$ degree for the volume calculation, implies that the area of spalling (A_s) in Equation 4 will be negative when the depth of spalling is less than 0.03 m. The depth of spalling cannot not be negative. It is not known if these equations can predict such small depths of spalling and hence these equations should only be used for depths of spalling greater than 0.03 m.

3.2.3 EXCEL code for evaluating the spalling hazard

Figure 3–7 illustrates the calculation logic used to establish the spalling factor of safety, the probability of spalling and the average depth of failure. It should be noted that the mean uniaxial compressive strength is used to establish the rock mass spalling strength (σ_{sm}), and the factor k is used to establish the range of rock mass spalling strength.

An EXCEL spreadsheet was developed for Figure 3–7 using Equations 1 and 3, i.e, spalling factor of safety and the depth of spalling, respectively (Figure 3–8). The probability for spalling and the potential range in the depth of spalling was determined using the software @Risk[4] which consists of a series of macros for EXCEL that conducts Monte Carlo simulations. In Figure 3–8 the function RiskTriang(min,mean,max) is used to represent a triangular distribution for the input parameter. An example of the input parameters, the calculation sequence used in EXCEL, and the output in graphical form are provided in Figure 3–8. The input parameters are site specific and for this example the data were for the deposition holes at a depth of 350 m.

The Factor of Safety in Figure 3–8 was calculated using the @Risk Monte Carlo simulations and hence the output is expressed as a probability distribution, shown graphically in Figure 3–8. For these simulations there is no correlation between stress and strength, i.e., the highest stress can be associated with the lowest strength. In reality, this may not be the case as the highest in-situ stresses are often found in the most competent rock mass and the lowest stresses in highly fractured rock masses. This level of information is currently not available, and for these analysis this issue is not addressed.

The output in Figure 3–8 for the spalling factor of safety provides the mean factor of safety as well as the probability of the factor of safety being less than 1. If there is 10% probability that the spalling factor of safety is less than 1, this implies that for a 100 m long tunnel, there is the potential that 10 m of the tunnel length will experience spalling. If there is 0% probability of spalling there is no depth of spalling. However, once the probability of spalling is greater than zero, a depth of spalling is determined. For the depth of spalling, only the mean depth of spalling was used for assessing the severity of the hazard.

[4] Available from www.palisade.com

Step 1: Stress and strength distribution

$\sigma_{sm} = k\ \mathrm{UCS_{mean}} =$ 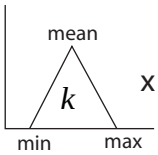

x $\mathrm{UCS_{mean}}$

$\sigma_{\theta\theta} = 3\sigma_1 - \sigma_3 =$ 3 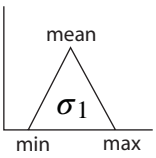

− 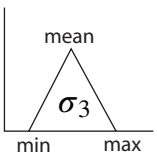

Step 2: Spalling Factor of safety

$\mathrm{FOS} = \frac{\sigma_{sm}}{\sigma_{\theta\theta}} =$ 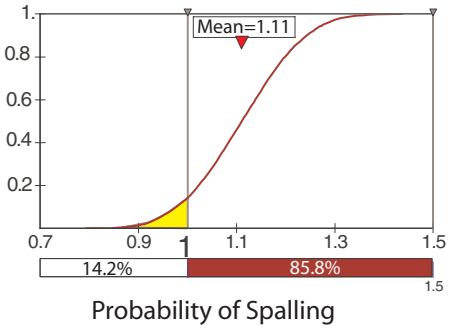

Step 3: Depth of spalling

$S_d = a\left(0.5\,\frac{\sigma_{sm}}{\sigma_{\theta\theta}} - 0.52\right)$

a = radius of the opening in metres

$S_d =$ 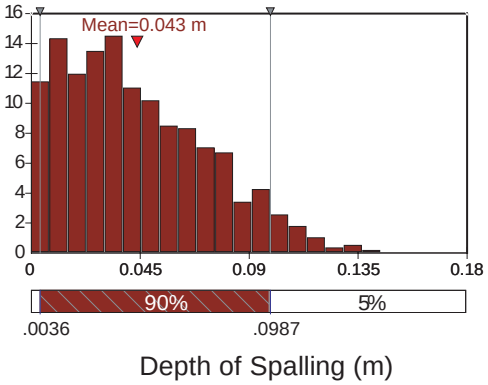

Figure 3–7: *Illustration of the calculation flow chart used to establish spalling factor of safety, the probability of spalling and the average depth of failure.*

	A	B	C	D	E	F
1	**INPUT PARAMETERS**					
2		Radius =	0.9	m		
3		Depth =	350	metre		
4				Min	Mean	Max
5		UCS =	Mean		225	
6		Shmax =	RiskTriang(D6, E6, F6)	E6-E6*0.1	35+0.02*C3	E6+E6*0.1
7		Shmin =	RiskTriang(D7, E7, F7)	E7-E7*0.1	17.5+0.01*C3	E7+E7*0.1
8		σsm/UCS =	RiskTriang(D8, E8, F8)	0.55	0.57	0.59
9						
10	**OUTPUT**					
11	Ratio= σsm/UCS					
12	Factor of Safety (FOS) = (Ratio*Mean UCS)/(3*Shmax-Shmin)					
31	Depth of Spalling =	RiskOutput() +IF(FOS<1,(rad(0.5*(3*Shmax-Shmin)/(Ratio*Mean UCS)-0.52),0)				

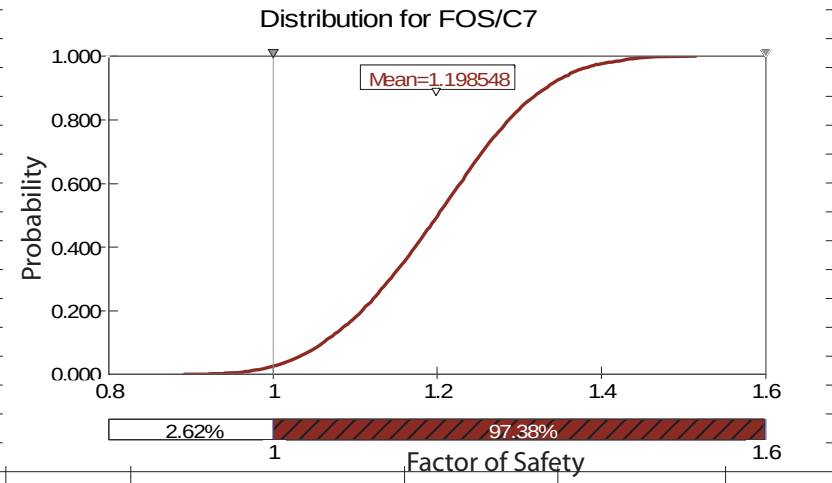

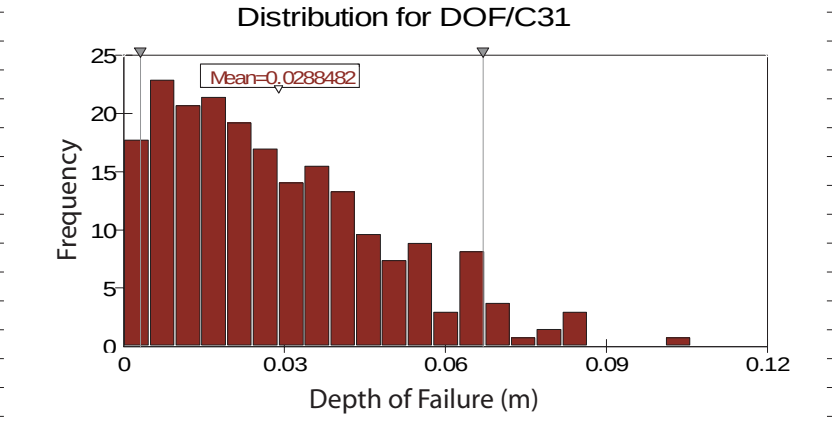

Figure 3–8: *Example of the spreadsheet code including the @Risk functions used to assess the Factor of Safety for spalling and the associated depth of failure. This fictitious example is for deposition holes at a depth of 350 m.*

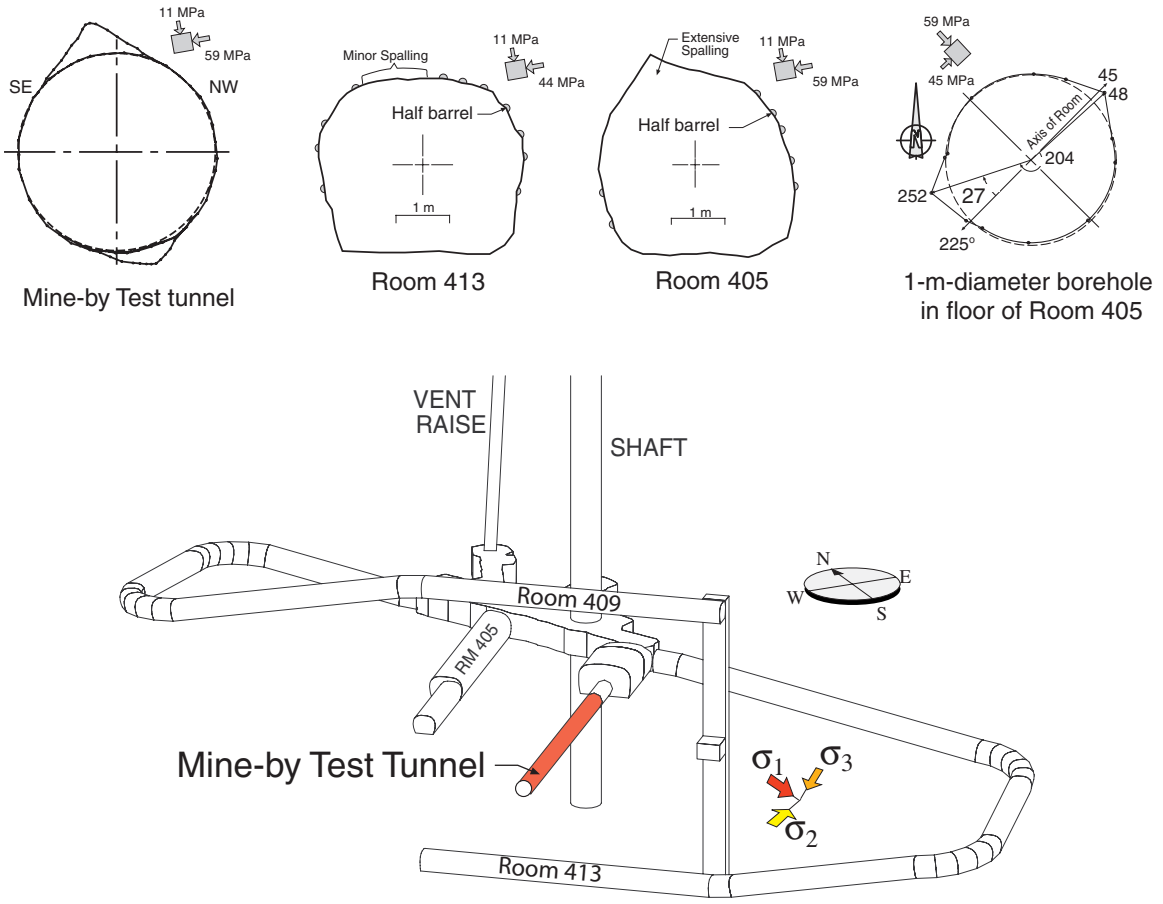

	σ_1	σ_2	σ_3
Magnitudes (MPa)	60±3	45±4	11±4
Trend/Plunge (°)	145/11	054/08	290/77

Figure 3–9: *Location of AECL's Mine-by test tunnel, Room 413, Room 405 and 1-m-diameter borehole drilled from the floor of Room 405.*

3.2.4 Calibration of methodology

The 420 Level of AECL's URL provided an opportunity to calibrate the methodology used in this report. The extent of spalling, indicated by the size of the v-shaped notch, varied for tunnels in different directions. Figure 3–9 shows the location of various tunnels on the 420 Level of AECL's URL, the observed spalling and the orientation of the in-situ stress magnitudes. The extent of spalling can be readily seen in Figure 3–9 by comparing the excavation profiles for Room 413 and Room 405. Note that for Room 413, which is oriented parallel to the maximum horizontal stress, only very minor spalling occurred as the half-barrels associated with the blast holes were still visible for nearly all of the perimeter profile. While Room 405 which was excavated perpendicular to the maximum principal stress, showed extensive spalling, i.e., large v-shaped notch. In addition to the AECL data, an additional calibration analysis was carried out for the 5-m-diameter TBM tunnel used in SKB's Prototype Repository (see Figure A.5 for location). No spalling was observed during the excavation of this tunnel.

Note that Martin and Read /1996/ established the confidence for the in-situ stress tensor for the URL 420 Level through large scale back-analyses and provided the likely range in stress magnitudes. These ranges were used in conjunction with the approach given in Figure 3–7 to determine the probability of spalling for the AECL's Mine-by test tunnel, Room 413 Level and AECL's 1-m-diameter borehole drilled from the floor of Room 405 (Figure 3–10a). The same approach was also used for the Äspö Prototype Repository Tunnel using the stress tensor determined from convergence back analysis by Andersson and Martin /2003/. The computed mean factors of safety for spalling are in agreement with the observations. For example, in AECL's Room 413 the methodology indicated a mean Factor of Safety of 0.99, which is in agreement with the very minor spalling observed. However the tunnels oriented perpendicular to the maximum stress, which always exhibited spalling, had a mean factor of safety of 0.72. In addition there was no evidence of spalling in the Äspö Prototype Repository tunnel which is also consistent with the computed mean factor of safety of 1.43. The range in the factors of safety computed in Figure 3–10a have been summarized in Figure 3–10b.

A circular access tunnel for the Äspö Pillar Stability Experiment while not shown on Figure 3–10b would have had a Factor of Safety of approximately 1.5, similar to that computed for the Äspö Prototype Repository tunnel. By modifying the tunnel geometry to increases the tangential stresses on the tunnel rook and floor the factor of safety was reduced to 1.3. Though the factor of safety was significantly decreased no spalling was observed in the 50-m-long tunnel. However, by drilling the 1.8-m-diameter borehole in the floor of the tunnel the tangential stresses on the the boundary of the borehole locally exceeded the spalling strength and the factor of safety was reduced to approximately 1. By drilling the second 1.8-m-diameter borehole the tangential stresses were increased again and spalling was observed over 25% of the borehole depth (see Figure 3–3b). The computed factor of safety based on elastic stresses would have decreased to approximately 0.8 at the end of drilling the second hole. While the Äspö Pillar Stability Experiment was not used in the development of Figure 3–10b the spalling observations and the computed elastic stresses reported by Andersson /2005/ are consistent with the trend in Figure 3–10b.

Inspection of Figure 3–10b reveals that if the mean Factor of Safety is greater than approximately 1.15, the probability of spalling is essentially zero. In these analyses the in-situ stress tensor is known with confidence. During the early stages of a site investigation program the in-situ stress tensor may not be known with the same degree of confidence as the examples used to develop Figure 3–10b. Hence it is suggested that when the stress tensor is not well constrained a spalling Factor of Safety of 1.25 be used for preliminary design purposes. Based on Figure 3–10b a mean Factor of Safety of 1.25 should give a probability of spalling of approximately zero.

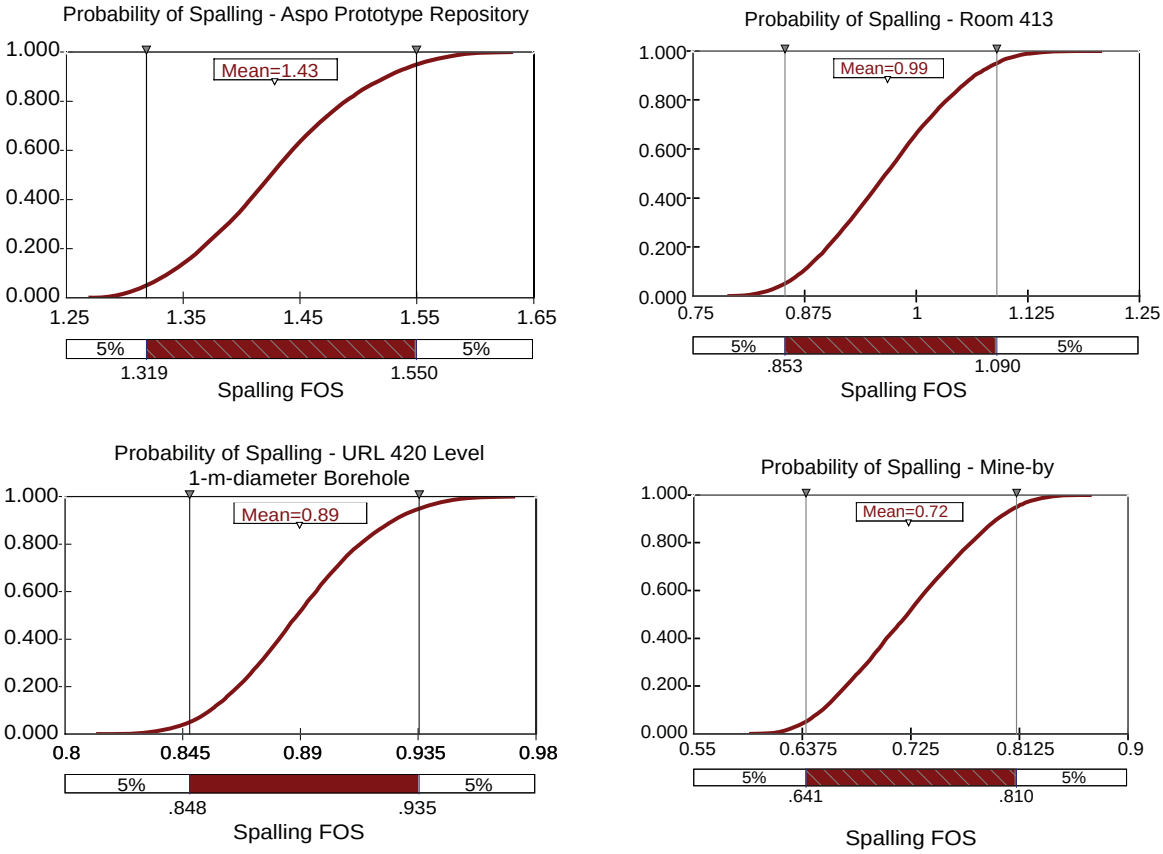

(a) Probability of spalling

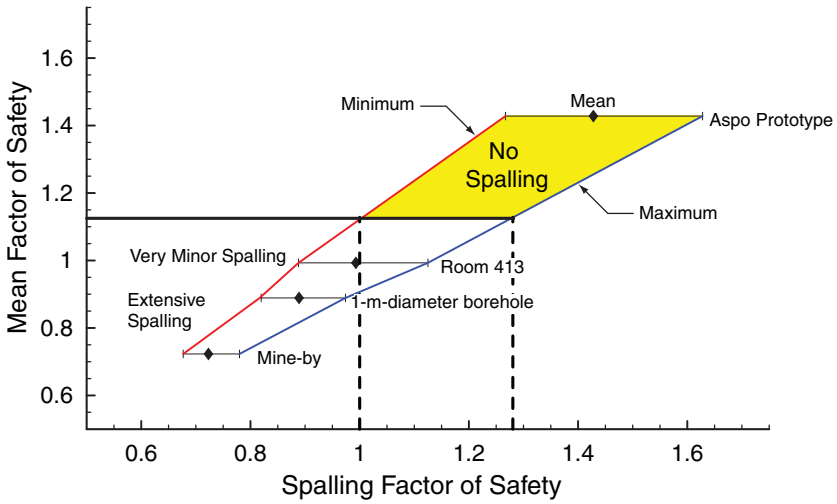

(b) Spalling factor of safety

Figure 3–10: *Comparison of the probability of spalling and the factor of safety for the Äspö Prototype Repository Tunnel, AECL's Mine-by test tunnel, Room 413 and 1-m-diameter borehole drilled from the floor of Room 405.*

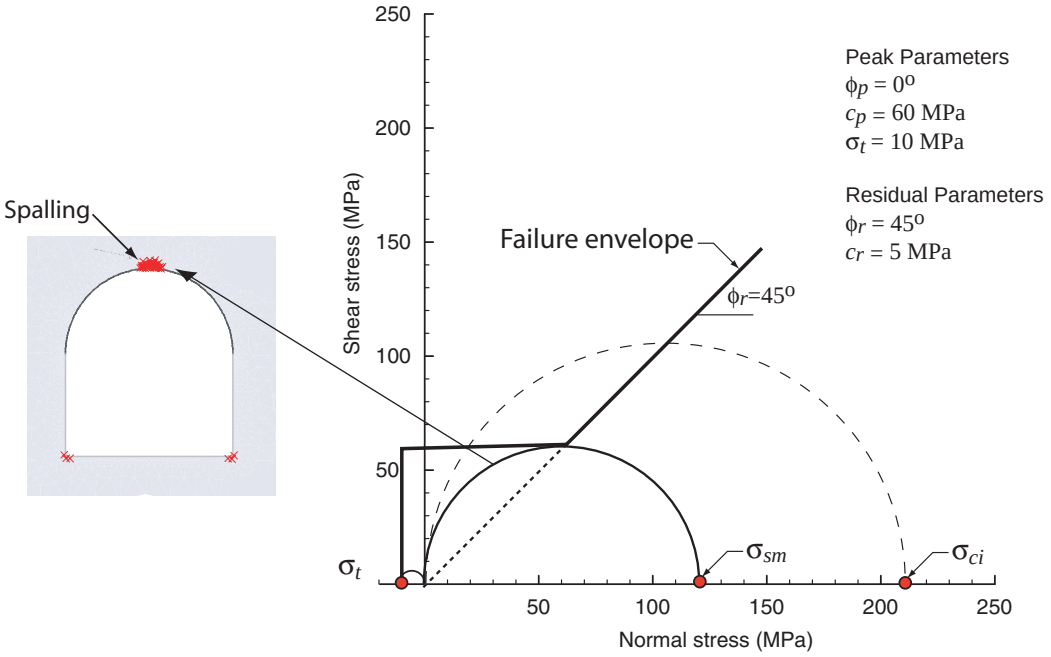

Figure 3–11: *The spalling failure criterion developed by Martin et al. /1999/ and Hajiabdolmajid et al. /2002/ for implementation in numerical continuum software such as Phase2 or Flac.*

3.3 Spalling for noncircular openings

The methodology used to assess the spalling hazard given in the previous sections was for a single circular opening in a continuous, homogeneous, isotropic, linearly elastic rock. For non-circular openings or when the interaction of multiple openings must be evaluated, a numerical analysis is required. Appendix A describes the development of the spalling criteria that should be used for numerical analysis. This criteria uses a Mohr-Coulomb failure envelope with the peak friction angle (ϕ_p) set to zero, to indicate that the strength of the rock is entirely cohesive and the peak cohesion (c_p) of the rock set to 1/2 the spalling rock mass strength ($c_p = 60$ MPa). Once spalling occurs and the slabs form, the strength of the broken rock slabs is mainly frictional and hence the c_r is set to a nominal 5 MPa reflecting the small strain nature of the problem, and ϕ_r is set to 45°. The peak tensile strength (σ_t) goes to zero once spalling initiates.

Figure 3–11 shows the spalling-failure envelope that could be used to predict the depth and extent of spalling using the finite element program Phase2[5]. Hajiabdolmajid et al. /2002/ and Hajiabdolmajid et al. /2003/ show how the failure criterion in Figure 3–11 can be implemented in Flac[6]. Once the depth of spalling has been assessed using this approach, the length and capacity of support system can be determined assuming that the entire weight of the spalled region must be retained by the support.

3.4 Spalling and thermally-induced stresses

At a nuclear waste repository, thermal stresses will develop in the rock mass after the waste is placed. These thermal stresses will cause an increase in the tangential stresses on the

[5]www.RocScience.com
[6]www.itascacg.com

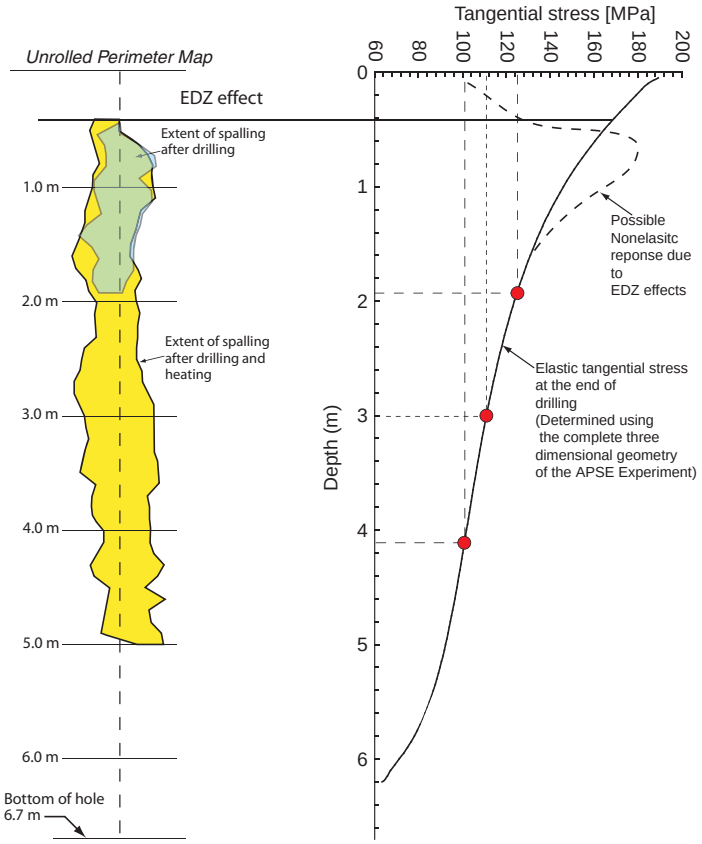

Depth (m)	Geometry stress (MPa)	Thermal stress (MPa) (E=55 GPa)	Spalling strength (MPa)
1.95	125	0*	125
3.0	111	13 – 15	124 – 126
3.55	106	24	130
(4.1	101	21	122)

*Prior to heating

Figure 3–12: *The rock mass spalling strength determined for the Äpsö Pillar Stability Experiment for geometry-induced stresses and for combined geometry and thermally-induced stresses.*

boundary of the underground openings. Hence, underground openings that are stable at the end of the excavation phase may become unstable during the heating phase, if the tangential stresses reach the rock mass spalling strength. One of the objectives of the Äpsö Pillar Stability Experiment was to evaluate the rock mass spalling strength under the conditions of thermal loading. Figure 3–12 shows the results from this experiment[7]. The results indicate that the average rock mass spalling strength is 125 MPa regardless of whether the tangential stresses are induced by geometry or by combined geometry and thermally induced stresses. Because these results are preliminary, the rock mass spalling strength given in Table 3–2 was used in this report for the spalling analyses reported in the following sections.

[7]Results presented by C. Andersson (SKB) during the Äpsö Pillar Stability Experiment Meeting June 20 2005 at Äpsö

4 Forsmark analysis

4.1 Input data

4.1.1 Joint orientation and strength

The Discrete Fracture Model (DFN) in R-04-15 gave the following major joint sets (see Table 5-24 in R-04-15):

Table 4–1: Joint sets obtained from Discrete Fracture Model

	Joint Label	Dip Direction (°)	Dip (°)
1	North-East	313	89
2	North-West	216	87
3	North-South	265	87
4	East-West	187	87
5	Sub-Horizontal	330	11

4.1.2 In-situ stress

In-situ stress data for this report was based on the results contained in Sjöberg /2004/ and Carlsson and Christiansson /1986/. Those results are graphically shown in Figure 4–1.

The stress gradients illustrated in Figure 4–1 were taken from SKB's Site Description Model 1.2 and used to determine the stress magnitudes at the 350, 450, 550 and 650 m depths in Table 4–2. At present, there is uncertainty in the horizontal stress gradients below a 500 m depth. Table 4–2 presents the mean stress gradient as well as the uncertainty in the gradient based on all available data from the Forsmark site and the author's experience. For example, it is highly unlikely the vertical stress gradient will have a large variation with depth while there is considerable uncertainty in the minimum horizontal stress gradient with depth, expressed as $\pm 0.005z$ MPa/m and $\pm 20\%$, respectively in Table 4–2. This uncertainty is also shown graphically in Figure 4–1.

The maximum horizontal stress was determined from the recent Borre probe results given in Sjöberg /2004/. The higher horizontal stress magnitudes reported by Carlsson and Christiansson /1986/ for borehole DBT-1 in Figure 4–1 have not been included in developing the maximum horizontal stress gradient, because of the limitation in the data collection used at that time, i.e., only before and after measurements were taken. Hence, it is possible that the maximum horizontal stress gradient may be higher than that shown in Table 4–2. This will have to be checked in a future stress measurement program at Forsmark.

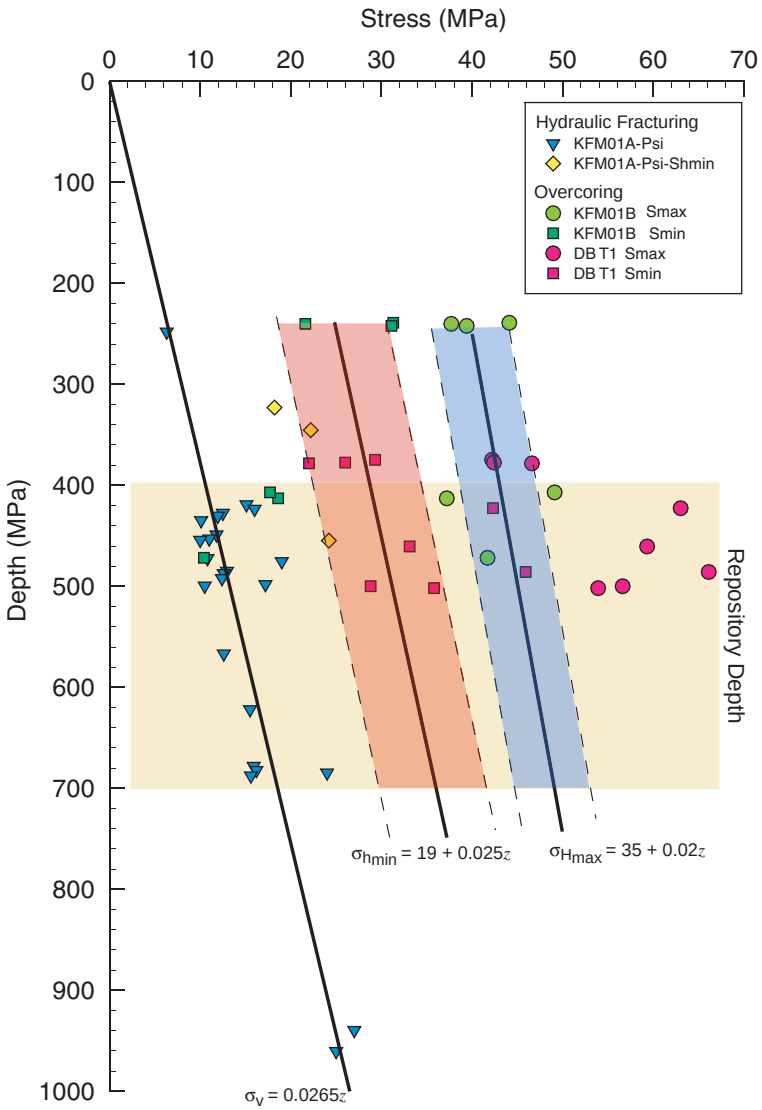

Figure 4–1: *Stress gradients compiled from overcoring Sjöberg /2004/and Hydraulic fracturing results.*

Table 4–2: Forsmark stress gradients used for spalling analysis.

Gradient (MPa/m)	σ_{Hmax} $35 + 0.02z$	σ_{hmin} $19 + 0.025z$	σ_{vert} $0.0265z$
Variability	$\pm 10\%$	$\pm 20\%$	$\pm 0.0005z$
Depth, z (m)	(MPa)	(MPa)	(MPa)
350	42	28	9.3
450	44	30	11.9
550	46	32	14.6
650	48	35	17.2

4.1.3 Uniaxial Compressive Strength

The uniaxial compressive strength were taken from laboratory test results from SKB SDM 1.2 SKB /2005a/. The data are summarized in Appendix B and shown graphically in Figures 4–2 and 4–3. Also shown on Figure 4–3 is the P-wave velocity. These velocities were measured on the core and can be used as an indicator of stress-induced damage i.e., microcracking, Martin and Stimpson /1994/. Notice that there is essentially no change in p-wave velocity above 450 m depth, suggesting that the stress magnitudes are not sufficient to induce microcracking.

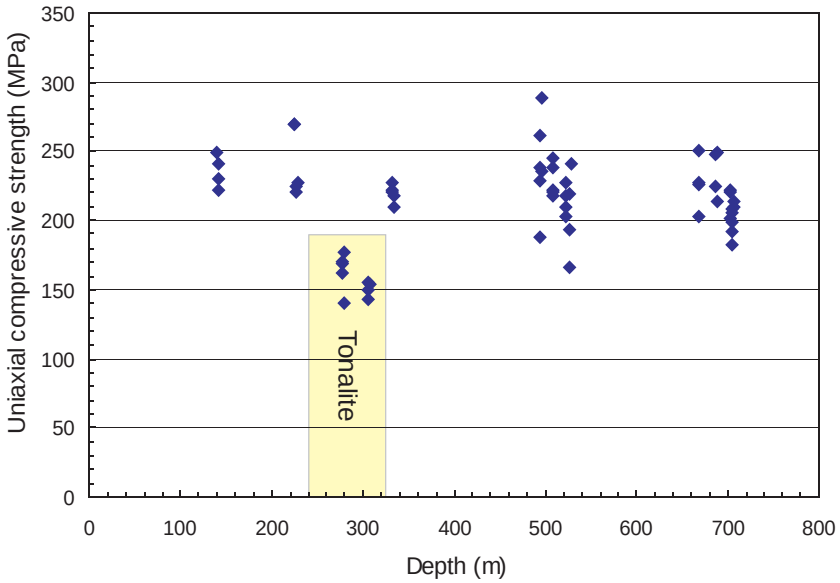

(a) UCS versus depth

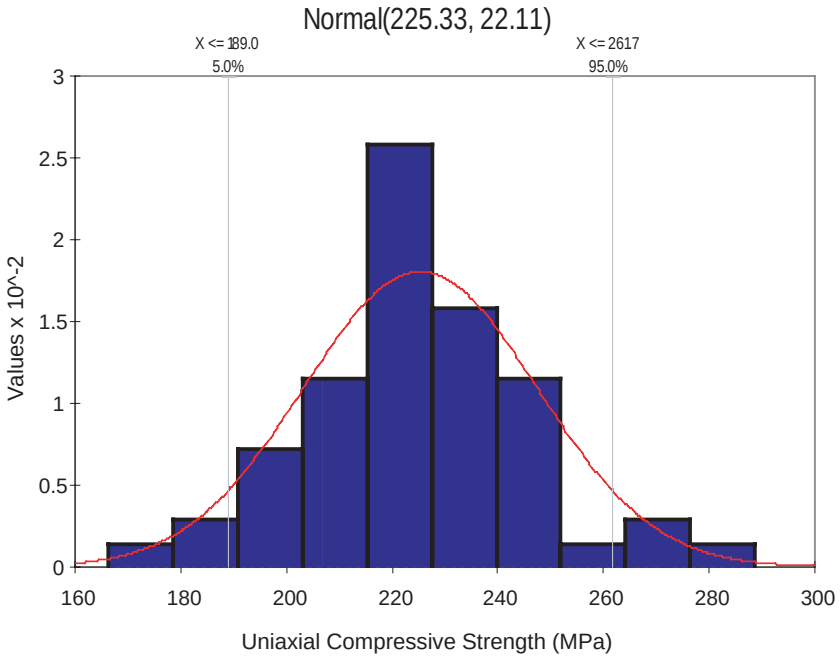

(b) UCS histogram

Figure 4–2: *Uniaxial compressive strength (UCS) versus depth from ground surface (top figure) and normal distribution fit to all the unconfined compressive strength data (Appendix B) for Forsmark rock unit. Tonalite has been excluded in the normal distribution.*

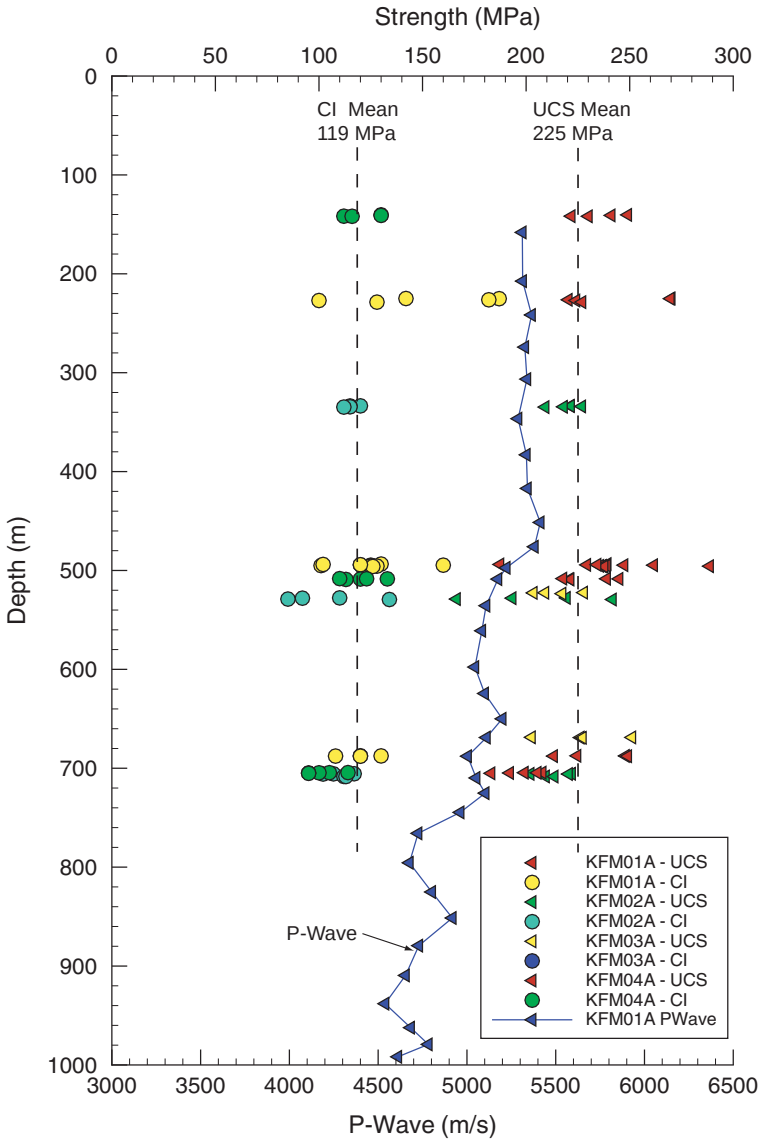

Figure 4–3: *Uniaxial compressive strength (UCS) and the onset of dilation (Crack Initiation - CI) versus depth. Also shown is the P-Wave velocity for KFM01A. The decrease in P-wave velocity below a depth of 500 m may be indicative of the development of stress-induced microcracks in the core.*

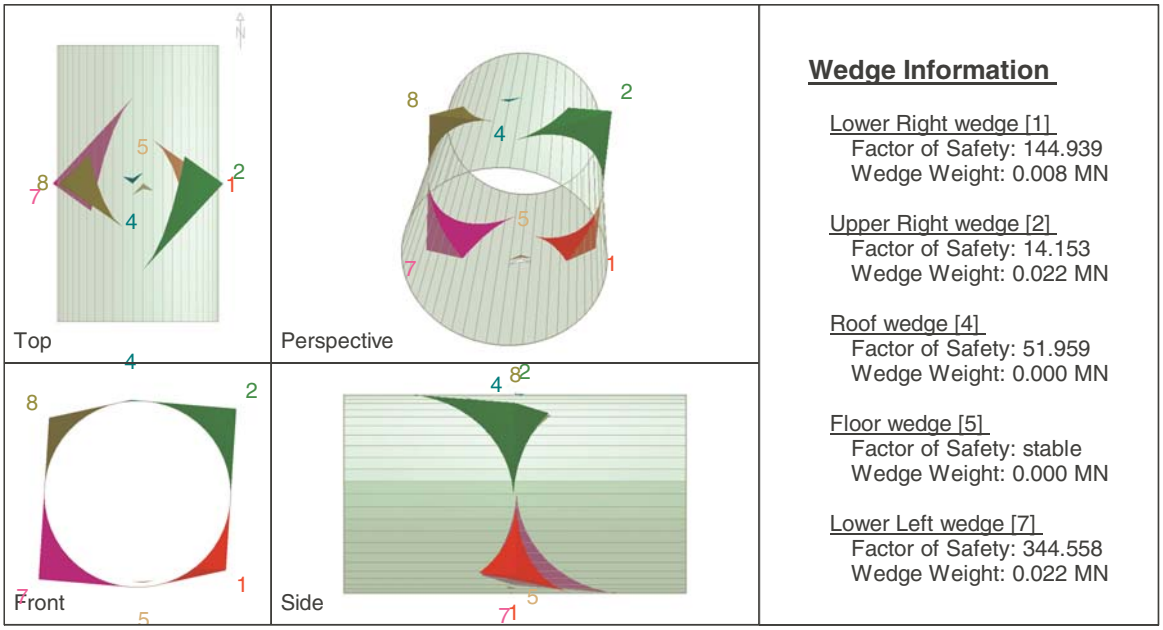

Figure 4–4: *Illustration of the perimeter wedges formed when the Deposition Tunnel is aligned to North (0 degrees).*

4.2 Wedge stability

Wedge analyses were carried out using the Discrete Fracture Network Model for Forsmark. A typical example is provided in Figure 4–4 and shows all the perimeter wedges that can potentially form when the horizontal 5-m-diameter tunnel is aligned to North (0 degrees). Figure 4–5 shows the maximum wedge weight as the tunnel is rotated 360 degrees in 10 degree increments. The spikes in these plots indicate that the worst orientation for the tunnel would be when it is approximately parallel to the strike of the sub-horizontal joint set, i.e. for a tunnel at 60 or 240 degrees trend. For this analysis only the tunnel trend was varied, all other parameters were kept constant. Also shown in Figure 4–5 is the minimum factor of safety when stress is not included in the analysis and support is neglected. For comparison purposes analysis were also carried out including the effect of in-situ stress (Figure 4–5). It is important to note that in-situ stress can have a significant stabilising effect on underground wedges and therefore should be included when conducting wedge analyses.

The results in Figure 4–5 indicate that all the wedges were stable or can be supported with nominal rock support, which is in agreement with tunnelling experience in the good quality rock of the Scandinavian shield. Hence wedge stability should not significantly influence design decisions related to repository depth or tunnel orientation.

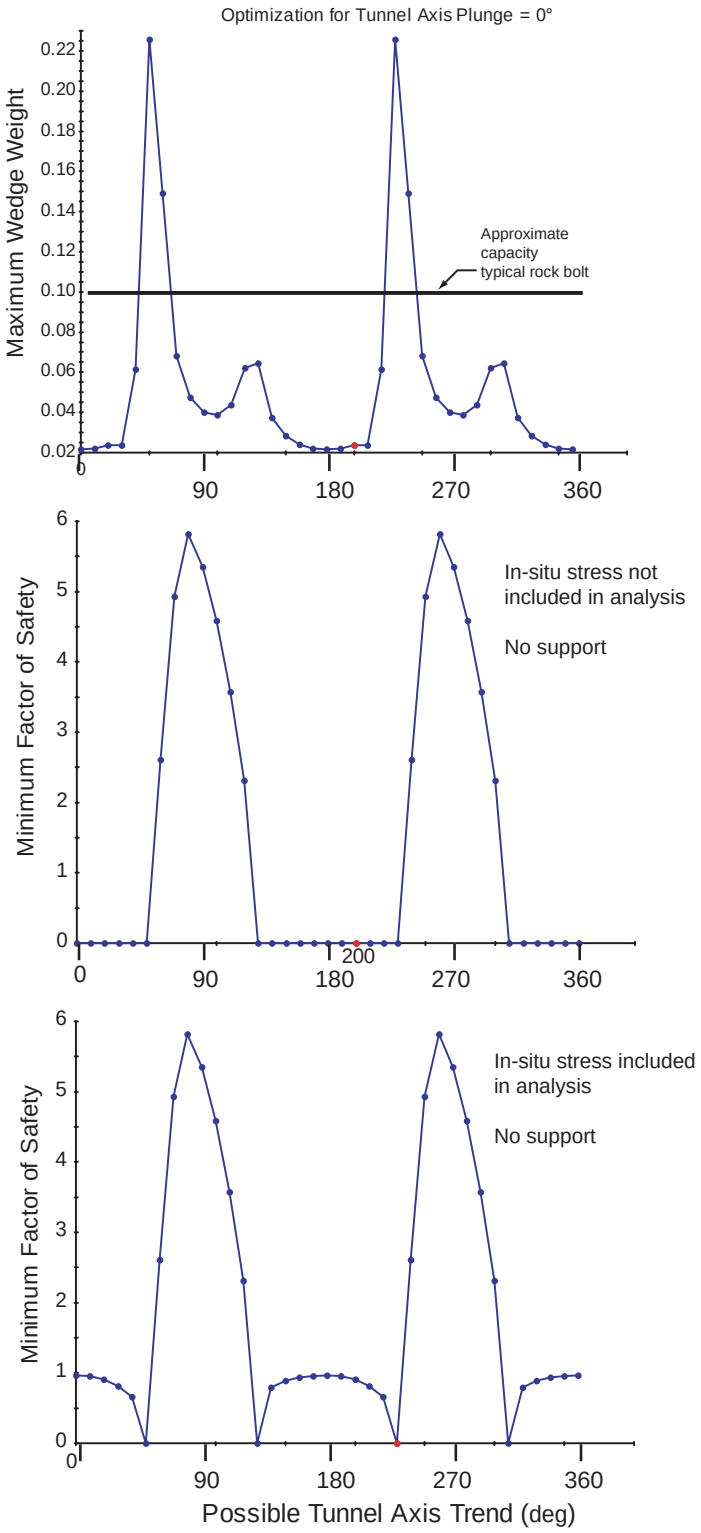

Figure 4–5: *Maximum weight of potential wedges as a function of tunnel trend and the minimum factor of safety. Note that the large wedges are stable and that all the small wedges would be handled by typical tunnel support.*

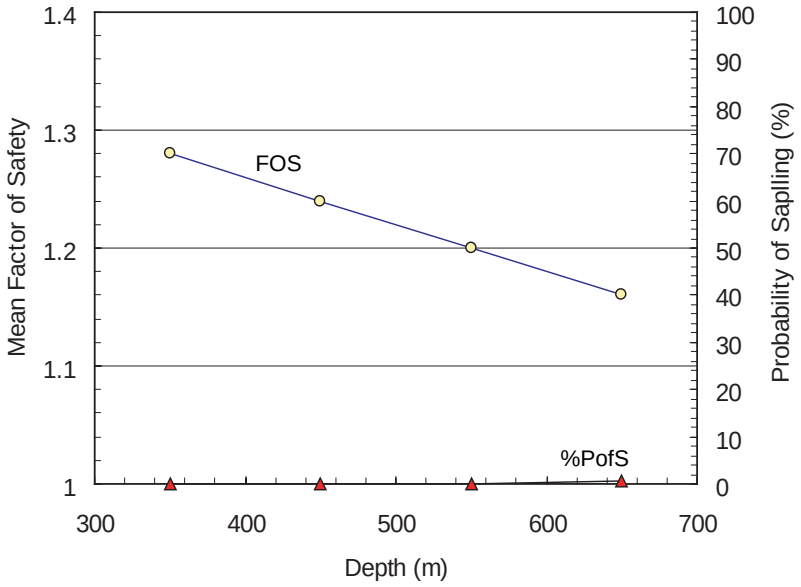

Figure 4–6: *Forsmark deposition holes - Mean Factor of Safety for spalling and the probability for spalling for repository levels at 350, 450, 550 and 650 m. Note that below a depth of 500 m there is less confidence in the in-situ stress magnitudes used in the analysis.*

4.3 Spalling stability

The spalling analysis was carried out using the spreadsheet functions shown in Figure 3–8. The detailed results from the analyses for both the deposition boreholes and the deposition tunnels are presented in terms of the mean factor of safety (see Equation 1), the probability in percent that the factor of safety is less than 1, and the associated mean depth of failure.

4.3.1 Vertical Deposition Holes

The mean factor of safety and probability for spalling for the 1.8-m-diameter vertical deposition boreholes at repository depths of 350, 450, 550 and 650 m are given in Figure 4–6. These results are based on 10,000 simulations using the @Risk software described in Figure 3–8. A probability of failure of 0%, implies that none of the 10,000 simulations had a factor of safety less than 1. At a depth of 650 m the probability of spalling is less than 1%. Hence these results suggest that spalling will not be encountered along the deposition holes, regardless of the repository depth.

It should be noted that these analysis assumes a uniform stress distribution along the deposition hole. In reality the deposition holes are 8-m long and connected to a Deposition tunnel. Hence the stress magnitudes along the deposition hole will not uniform. It is recommended that three dimensional stress analysis using the tunnel geometry and deposition hole spacing should be carried out in a later design phase for those cases where the probability of spalling is significant.

4.3.2 Deposition Tunnels

The factor of safety, probability for spalling and associated depth of failure in metres for the 5-m-diameter circular deposition tunnels at repository levels of 350, 450, 550 and 650 m is given in Figure 4–7. The tunnels are evaluated parallel (0deg), perpendicular

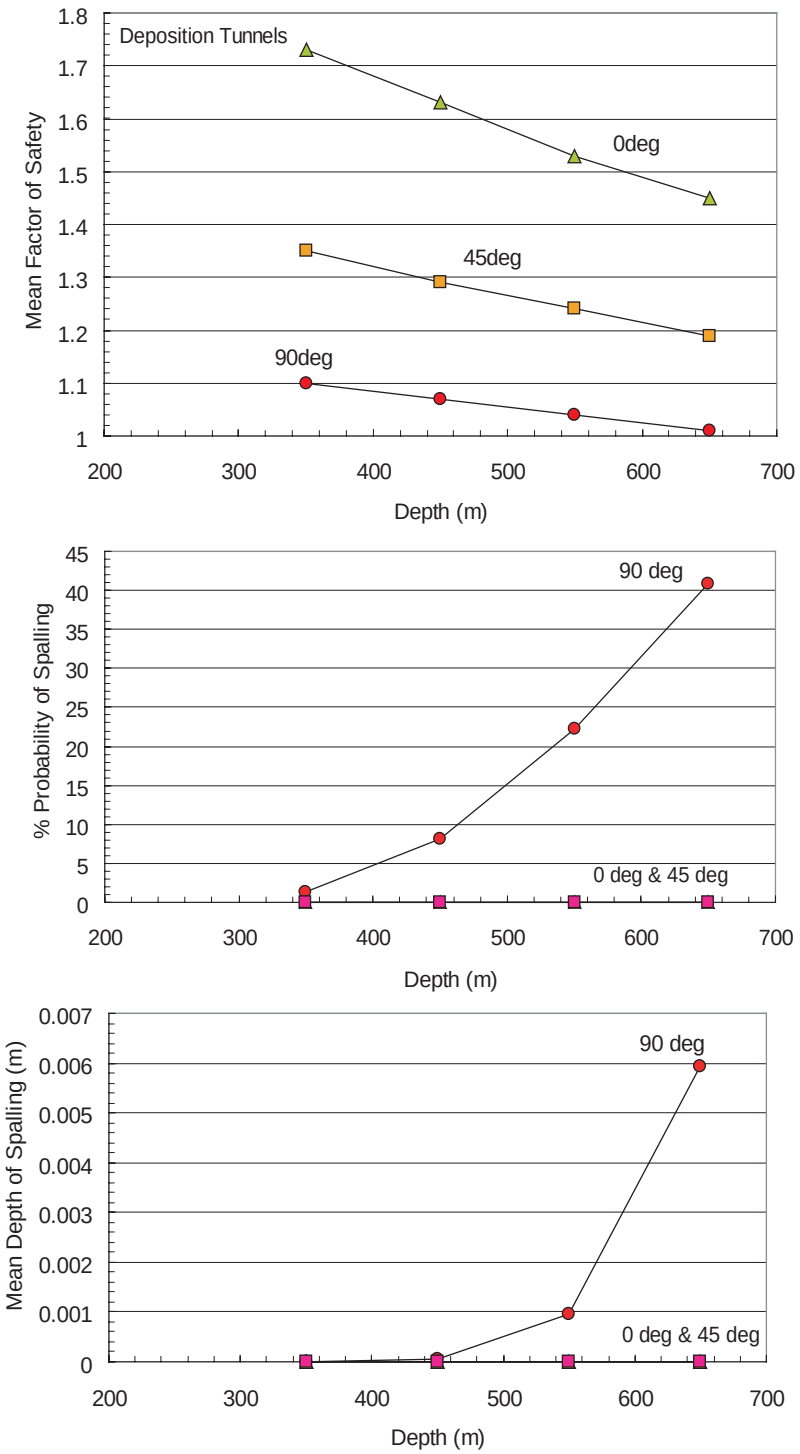

Figure 4–7: *Forsmark 5-m-diameter circular Deposition Tunnels - Factor of safety, Probability for spalling and associated depth of failure for repository levels at 350, 450, 550 and 650 m. The notation of 0 deg,45 deg and 90 deg, refers to the orientation of the deposition tunnel relative to the orientation of the maximum horizontal stress, i.e., 0 deg implies the tunnel is parallel to the maximum horizontal stress and 90 deg implies that the tunnel is perpendicular to the maximum horizontal stress.*

(90deg) and at 45 deg to the orientation of the maximum horizontal stress. Note that only the tunnels aligned perpendicular to the maximum horizontal stress has a significant risk for spalling. This risk increases with depth and the probability for spalling is approximately 40% at the 650-m depth.

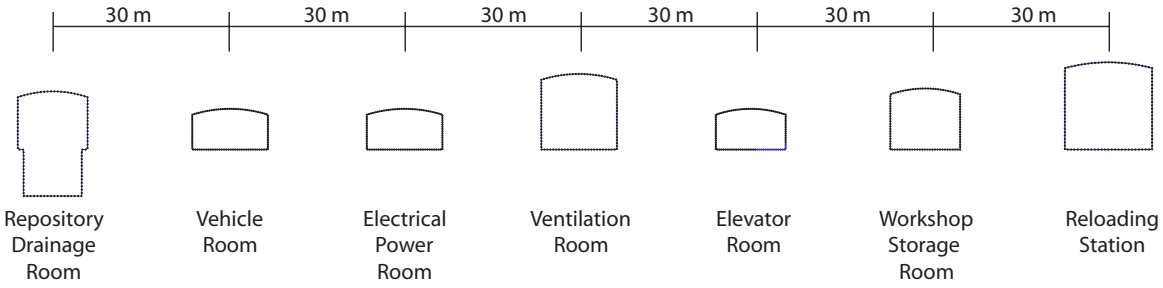

Figure 4–8: *Geometry and spacing of the tunnels used in the Central Area.*

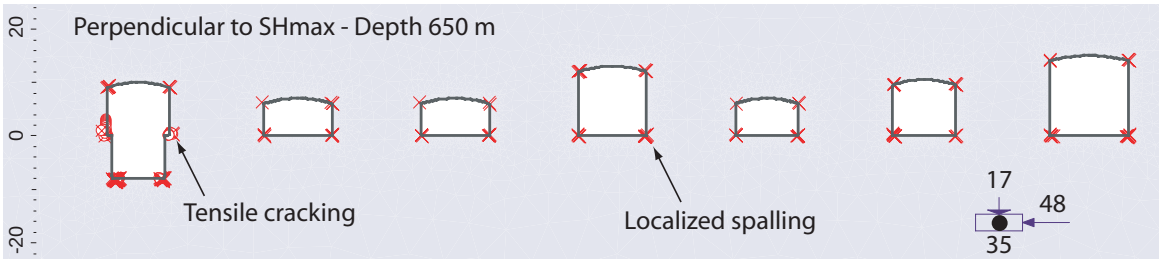

Figure 4–9: *Spalling around the common central area caverns at a repository depth of 650 m and the caverns oriented perpendicular to the maximum horizontal stress.*

4.3.3 Common central area caverns

A central area of the repository will be utilize a series of caverns with varying cross sections. These caverns and there relative spacing is shown in Figure 4–8.

Because the stresses around these tunnels cannot be determined using the Kirsch equations, spalling analyses were carried out using Phase2, the spalling criterion given in Table 3–2 and the failure envelope given in Figure 3–11. The results from the Phase2 analysis are given in Figure 4–9, and indicates that minor localized spalling may occur at the corners of the excavations where the stress magnitudes are elevated by the corner geometry. However, this is not considered significant and is seldom a problem in practice. As, with the deposition tunnels, this potential for spalling can be eliminated by orienting the tunnels parallel to the maximum horizontal stress.

When excavations, such as the repository drainage vault, have high flat walls the potential for tensile failure is elevated as shown in Figure 4–9. In practice, tensile failure is seldom observed as a single fracture surface. It often occurs as a diffuse zone of cracking, seldom requiring support. However, when joints occur in these flat sidewalls the potential for wedge failure is elevated significantly as the clamping stresses in sidewalls are significantly decreased. Replacement of these flat sidewalls with slightly curved sidewalls would improve stability. Such issues should be addressed during the detailed design phase.

Due to the importance of the central area during operations, it is anticipated that normal rock reinforcement (shotcrete and bolts) will be employed. It is anticipated that local instabilities can be handled by such reinforcement.

5 Simpevarp analysis

5.1 Input data

5.1.1 In-situ Stress

Two in-situ stress domains have been determined for the Simpevarp area[8] (Figure 5–1). These domains have been established using the overcore data in Figure 5–2.

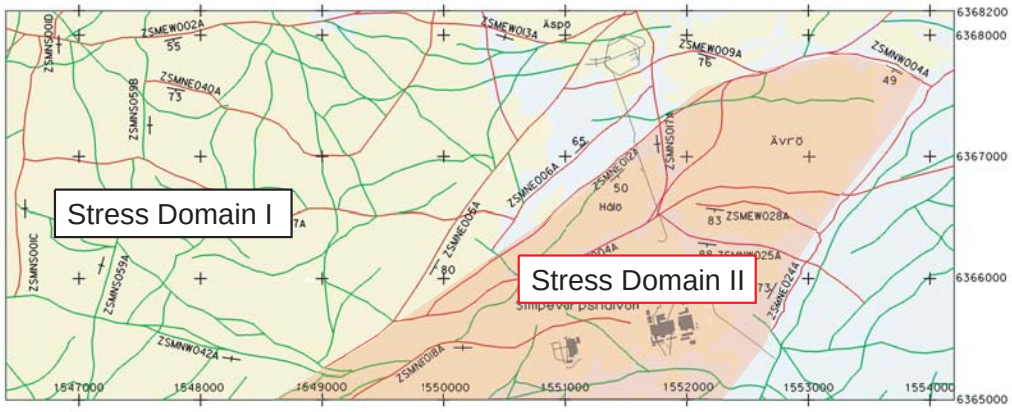

Figure 5–1: *Location of stress domains for Simpevarp area, (taken from Simpevarp SDM 1.2 SKB /2005b/).*

Table 5–1 gives the stress gradients used for the analyses in this report based on the data in Figure 5–2. At present there is considerable uncertainty in the gradient for the maximum horizontal stress in Stress Domain I. The uncertainty in the horizontal stress components was taken into account by assuming the mean stress given by the gradient ±25%. Hence a range of stress magnitudes was used in the analyses.

Table 5–1: In-situ stress gradients used for Simpevarp spalling analysis.

	Stress Domain I			Stress Domain II		
	σ_{Hmax}	σ_{hmin}	σ_{vert}	σ_{Hmax}	σ_{hmin}	σ_{vert}
Gradient (MPa/m)	$3 + 0.06z$	$0.019z$	$0.0265z$	$0.0314z$	$0.011z$	$0.0265z$
	±25%	±25%	$\pm 0.002z$	±15%	±15%	$\pm 0.002z$
Depth,z (m)	(MPa)	(MPa)	(MPa)	(MPa)	(MPa)	(MPa)
350	24	6.3	9.1	11	3.9	9.1
450	30	8.1	11.7	14.1	5.0	11.7
550	36	9.9	14.3	17.3	6.1	14.3
650	42	11.7	16.9	20.4	7.2	16.9

[8]Based on SKB - Simpevarp Site Description Model

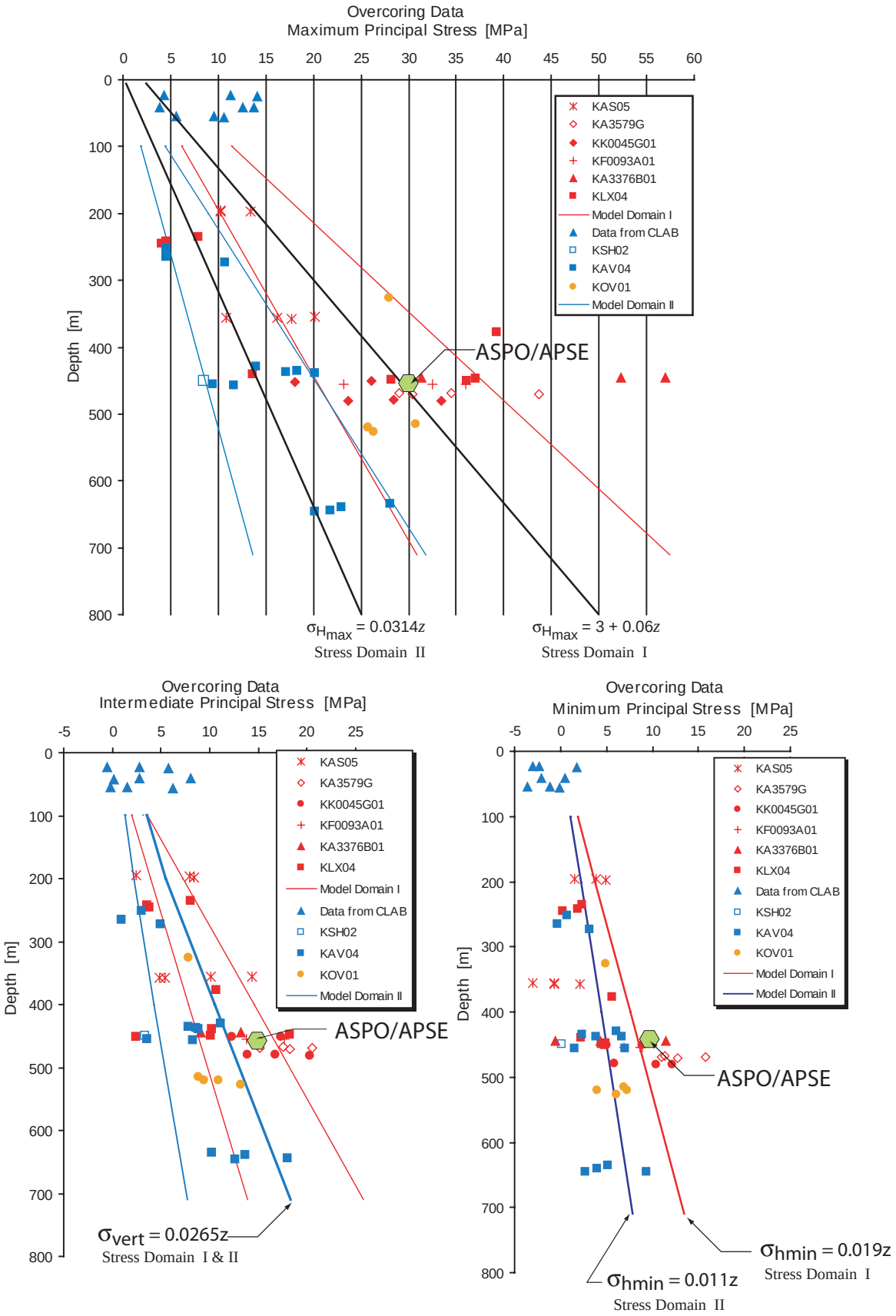

Figure 5–2: *Stress domains for Simpevarp area based on overcore test results, (data taken from Simpevarp SDM 1.2 SKB /2005b/).*

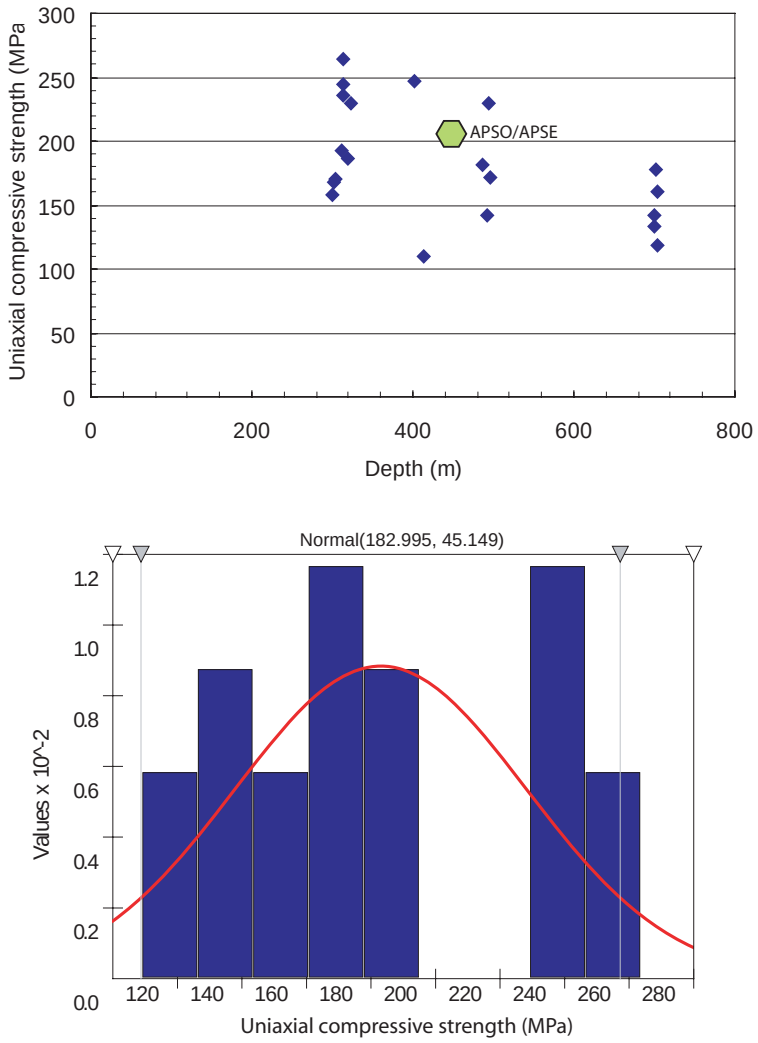

Figure 5–3: *Simpevarp: Uniaxial compressive strength (UCS) versus depth and a normal distribution fit to all the data. The large scatter in the UCS at depth is thought to be related to the large number of healed fractures in the samples tested.*

5.1.2 Uniaxial Compressive Strength

The uniaxial compressive strengths were taken from laboratory test results (see Appendix C) and summarized in POM 1.2. The data are shown graphically in Figure 5–3 and Figure 5–4. The data shows considerable scatter which is likely caused by the number of inclined healed fractures that were present in the core. Note that in Figure 5–4 the P-wave velocity decreases significantly below a depth of about 500 m. This decrease likely reflects the increase in microcracks with depth. In this case the microcracks are probably associated with the fracturing observed in the core, rather than increasing in in-situ stress magnitudes, as is normally assumed.

The rock mass spalling strength used for these analyses was taken as $0.57 \pm 0.02 \times$ UCS. Using a mean UCS $=$ 183 MPa, the rock mass spalling strength ranges from 100 to 108 MPa.

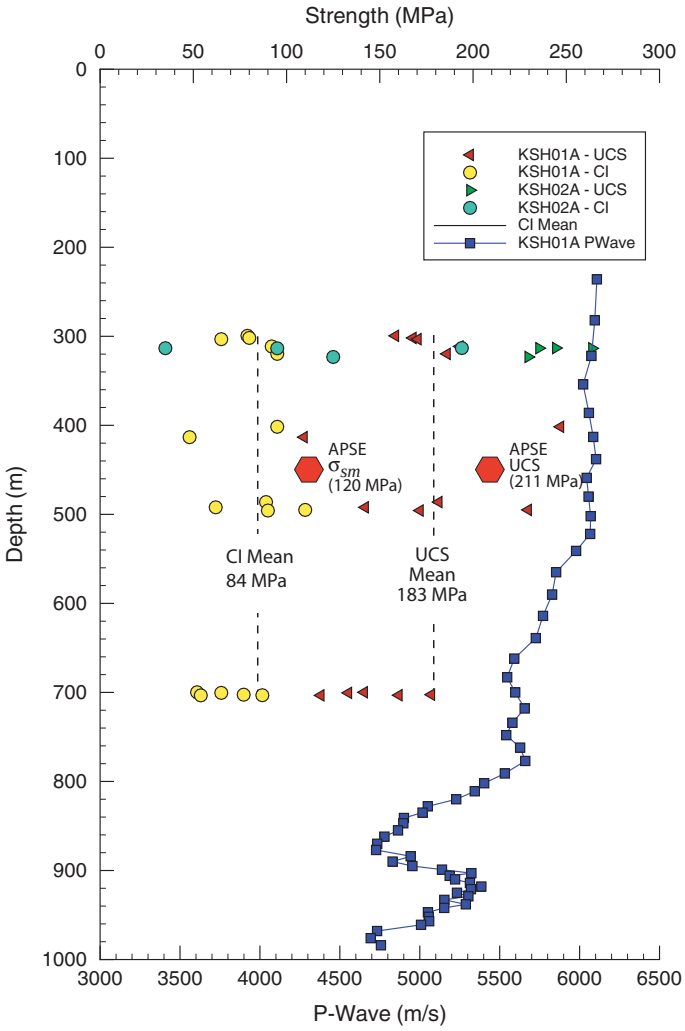

Figure 5–4: *Uniaxial compressive strength (UCS) and onset of dilation (Crack Initiation) versus depth. Also shown is the P-Wave velocity for Borehole KSH01A, the mean uniaxial compressive strength for Äpsö Diorite and the rock mass spalling strength obtained from the pillar stability experiment.*

5.2 Wedge stability

The results from Forsmark, indicated that the wedges encountered at the repository depth, based on the discrete fracture network model, could be adequately supported by the typical support system (shotcrete and bolts) used for tunnel construction in the Scandinavian Shield. The Äspö Hard Rock Laboratory has excavations to a depth of 450 m. The underground openings at Äspö HRL were supported with spot-bolts and shotcrete in localized areas, i.e., systematic application of support was not required. This construction experience in close proximity to the Simpevarp site suggests that wedge stability should also not be a significant issue at the repository depth at Simpevarp. This practical experience is considered more relevant at this stage of design then the results from wedge analyses based on the DFN model for Simpevarp. In addition there is some uncertainty with regard to the reliability of DFN model at the depth of the repository. This will be resolved as new information from the Site Characterisation program becomes available.

5.3 Spalling instability

The spalling analysis was carried out using the spreadsheet functions shown in Figure 3–8. The detailed results from the analyses for both the deposition boreholes and the deposition tunnels are given in following sections.

5.3.1 Vertical deposition holes

The results from the spalling analyses are summarized in Figures 5–5 and 5–6. These results indicate:

1. Stress Domain II: Spalling in the deposition holes will not be encountered regardless of repository depth.
2. Stress Domain I: The risk for spalling in the deposition holes increases below a repository depth of 450 m. At 550 m depth the probability of spalling is approximately 20% while at a repository depth of 650 m the probability for spalling increases to approximately 70%.

   It should be noted that if the rock mass is highly fractured the in-situ stress magnitudes maybe lower than magnitudes given for Stress Domain I. Hence the risk for spalling may be significantly reduced at depths below 500 m if the stress magnitudes are lower (e.g., see the results for Stress Domain II)

   Also shown on Figure 5–5 is the Factor of Safety for the deposition holes in the Prototype Repository located at a depth of 500 m in the Äspö Hard Rock Laboratory. The increase in the Factor of safety for the Prototype Repository occurs because of the increase in the UCS (211 MPa) and an increase in the minimum horizontal stress. It should be noted that no spalling was observed in the eight 1.8-m-diameter 8-m-deep deposition holes drilled for the Prototype Repository. These holes were spaced at 6-m centre-to-centre which is the typical spacing for the SKB KBS3 concept.

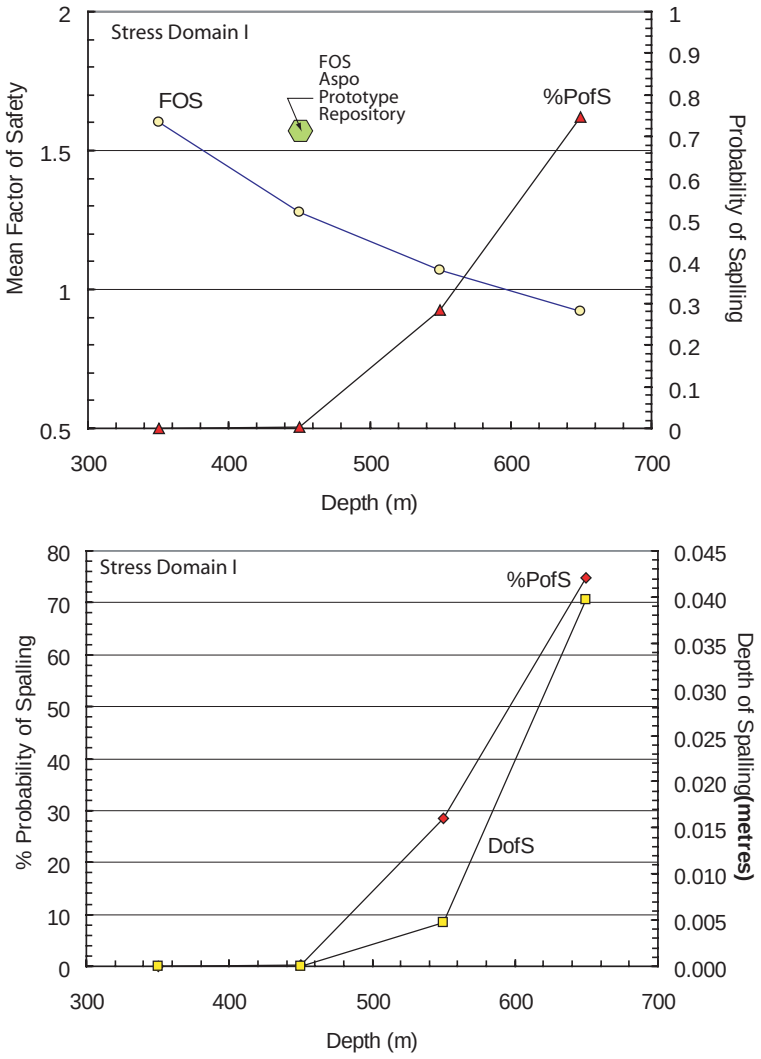

Figure 5–5: *Simpevarp: Spalling instability for vertical deposition holes for Stress Domain I.*

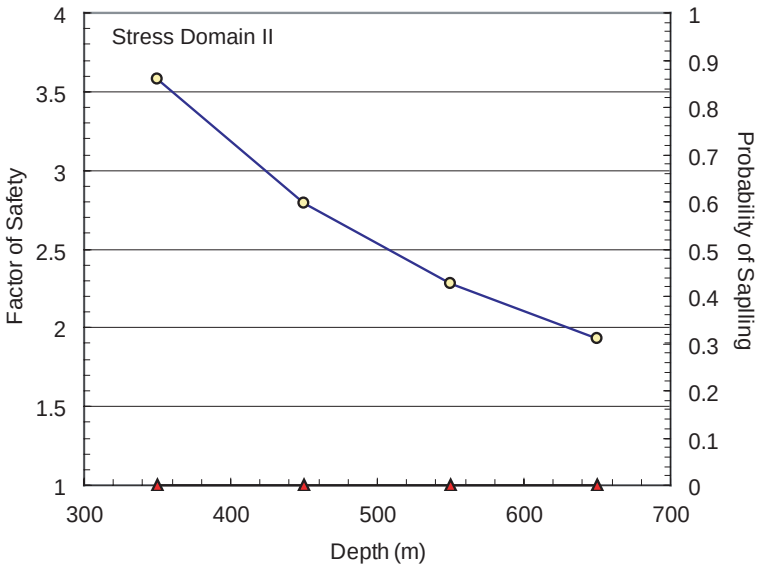

Figure 5–6: *Simpevarp: Spalling instability for vertical deposition holes for Stress Domain II.*

5.3.2 Deposition tunnels

The spalling analyses for circular Simpevarp deposition tunnels, for both Stress Domains I and II, are summarized in Figure 5–7. There is no probability of spalling in the deposition tunnels in stress Domain II at any depth or orientation. However, in Stress Domain I, the tunnels at 550 m and 650 m depth and oriented perpendicular to the maximum horizontal stress will likely encounter minor spalling. In Figure 5–7, the deposition tunnel in Stress Domain II orientated at 45 degrees to the maximum horizontal stress has the highest factor of safety against spalling. While in Stress Domain I the tunnels oriented parallel to the maximum horizontal stress have the highest factor of safety. Also shown in Figure 5–7-Stress Domain I, for reference purposes, is the Factor of safety for the spalling for the TBM tunnel at Äspö at a depth of 450 m. This tunnel is oriented approximately 30° from the maximum horizontal stress. No spalling was observed in the TBM tunnel, see Figure 5–8.

The analyses indicate that the probability for spalling in deposition tunnels for Stress Domain I at a depth of 650 m is greater than 50% when those tunnels are oriented perpendicular to the maximum horizontal stress. At a depth of 550 m the probability of spalling for these tunnels is reduce to approximately 10% (Figure 5–9). The relationship between the probability of spalling and the depth of spalling is also shown on Figure 5–9. At 550 m depth the average depth of spalling is 15 mm. This increases to 40 mm for a repository at a depth of 650 m.

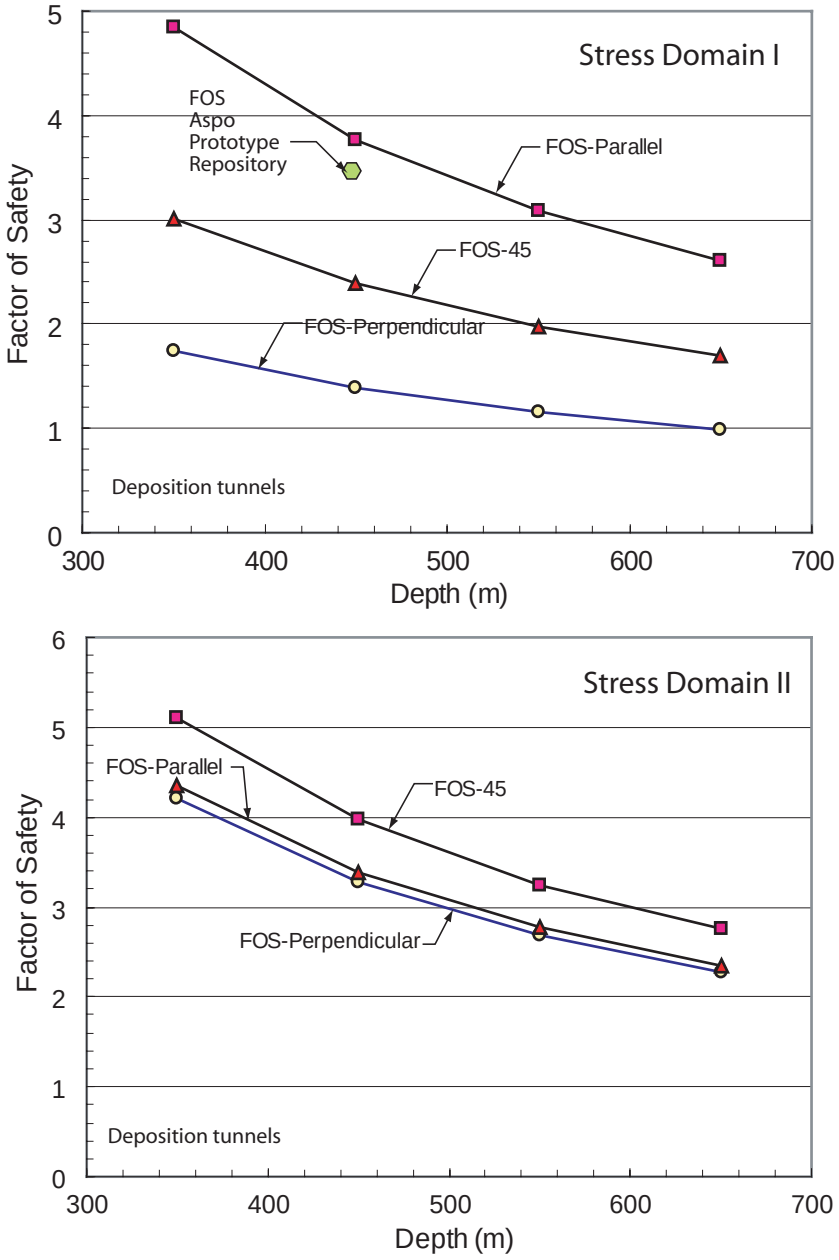

Figure 5–7: *Simpevarp: Spalling instability for deposition tunnels for Stress Domains I and II. Also shown, for reference purposes, is the the TBM tunnel at Äspö at a depth of 450 m. This tunnel is oriented approximately* 30° *from the maximum horizontal stress. No spalling was observed in the TBM tunnel, see Figure 5–8.*

Figure 5–8: *Example of the 5-m-diameter TBM tunnel profile at Äspö at a depth of 450 m. No spalling was observed in the TBM tunnel*

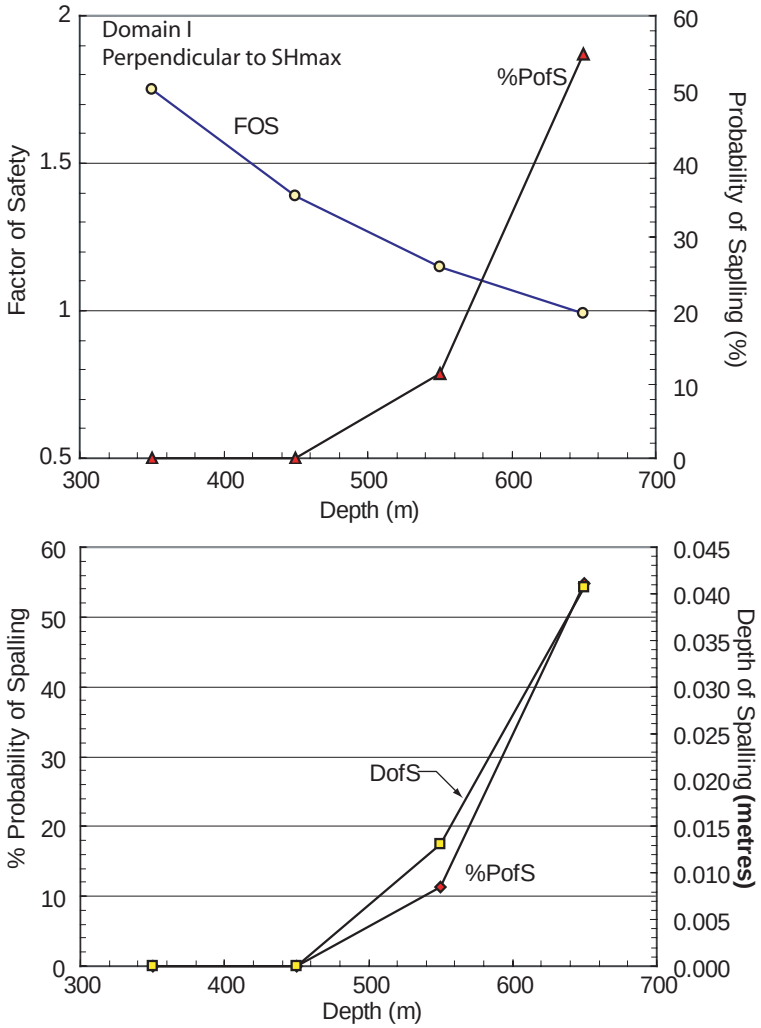

Figure 5–9: *Simpevarp: Spalling instability for deposition tunnels oriented perpendicular to the maximum horizontal stress in Stress Domain I.*

6 Laxemar analysis

6.1 Input data

Two in-situ stress domains have been determined for the Laxemar area[9]. A summary of the stress gradients given in the SDM 1.2 is given in Table 6–1.

The mean laboratory uniaxial compressive strength for the Granite to Quartz monzodiorite (Ävrö granite) is 195 MPa.

Table 6–1: In-situ stress gradients used for Laxemar spalling analysis.

	Stress Domain I			Stress Domain II		
Gradient (MPa/m)	σ_{Hmax} $5 + 0.058z$ $\pm 25\%$	σ_{hmin} $3 + 0.014z$ $\pm 25\%$	σ_{vert} $0.027z$ $\pm 0.002z$	σ_{Hmax} $0.032z$ $\pm 25\%$	σ_{hmin} $0.01z$ $\pm 25\%$	σ_{vert} $0.027z$ $\pm 0.002z$
Depth,z (m)	(MPa)	(MPa)	(MPa)	(MPa)	(MPa)	(MPa)
350	25.3	7.9	9.5	11.2	3.5	9.5
450	31.1	9.3	12.2	14.4	4.5	12.2
550	36.9	10.7	14.9	17.6	5.5	14.9
650	42.7	12.1	17.6	20.8	6.5	17.6

6.2 Wedge stability

The results from Forsmark, indicated that the wedges encountered at the repository depth, based on the discrete fracture network model, could be adequately supported by the typical support system (shotcrete and bolts) used for tunnel construction in the Scandinavian Shield. The Äspö Hard Rock Laboratory has excavations to a depth of 450 m. The underground openings at Äspö HRL were supported with spot-bolts and shotcrete in localized areas, i.e., systematic application of support was not required. This construction experience in close proximity to the Laxemar site suggests that wedge stability should not be a significant issue at the repository depth at Laxemar. This practical experience is considered more relevant at this stage of design then the results from wedge analyses based on the DFN model for Laxemar. In addition there is some uncertainty with regard to the reliability of DFN model at the depth of the repository. This will be resolved as new information from the Site Characterisation program becomes available.

6.3 Spalling instability

The spalling analysis was carried out using the spreadsheet functions shown in Figure 3–8. The detailed results from the analyses for both the deposition boreholes and the deposition tunnels are given in following sections.

[9]Based on SKB - Laxemar Site Description Model (SDM) 1.2

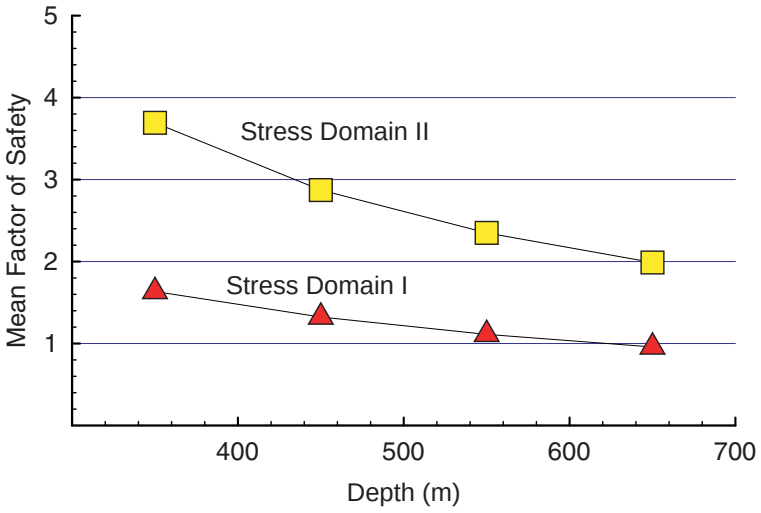

Figure 6–1: *Laxemar: Spalling instability for deposition holes in Stress Domains I and II.*

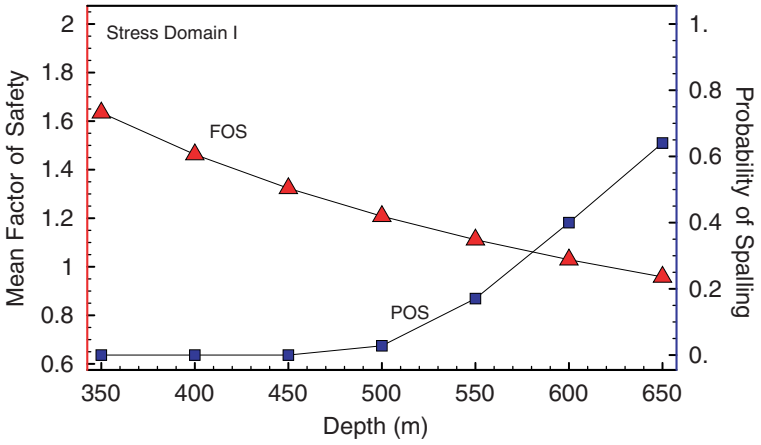

Figure 6–2: *Laxemar: Probability of spalling for deposition holes in Stress Domain I.*

6.3.1 Vertical deposition holes

The results from the spalling analyses for the vertical deposition holes are summarized in Figures 6–1 and 6–2. These results indicate:

1. Stress Domain II: Spalling in the deposition holes will not be encountered regardless of repository depth.
2. Stress Domain I: The risk for spalling in the deposition holes increases below a repository depth of 450 m. At 550 m depth the probability of spalling is approximately 20% while at a repository depth of 650 m the probability for spalling increases to approximately 60%.

6.3.2 Deposition tunnels

The spalling analyses for Laxemar circular deposition tunnels are summarized in Figure 6–4 for both Stress Domains I and II. There is no probability of spalling in the deposition tunnels in stress Domain II at any depth or orientation. However, in Stress Domain I, the deposition tunnels oriented perpendicular to the maximum horizontal stress

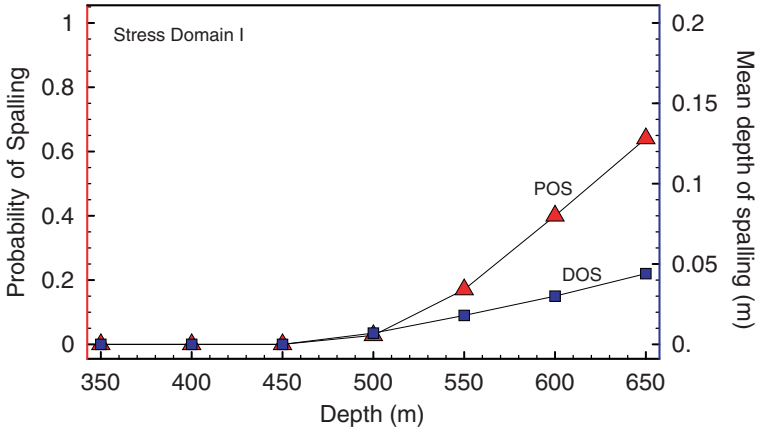

Figure 6–3: *Laxemar: Probability of spalling for deposition holes in Stress Domain I and the corresponding depth of spalling.*

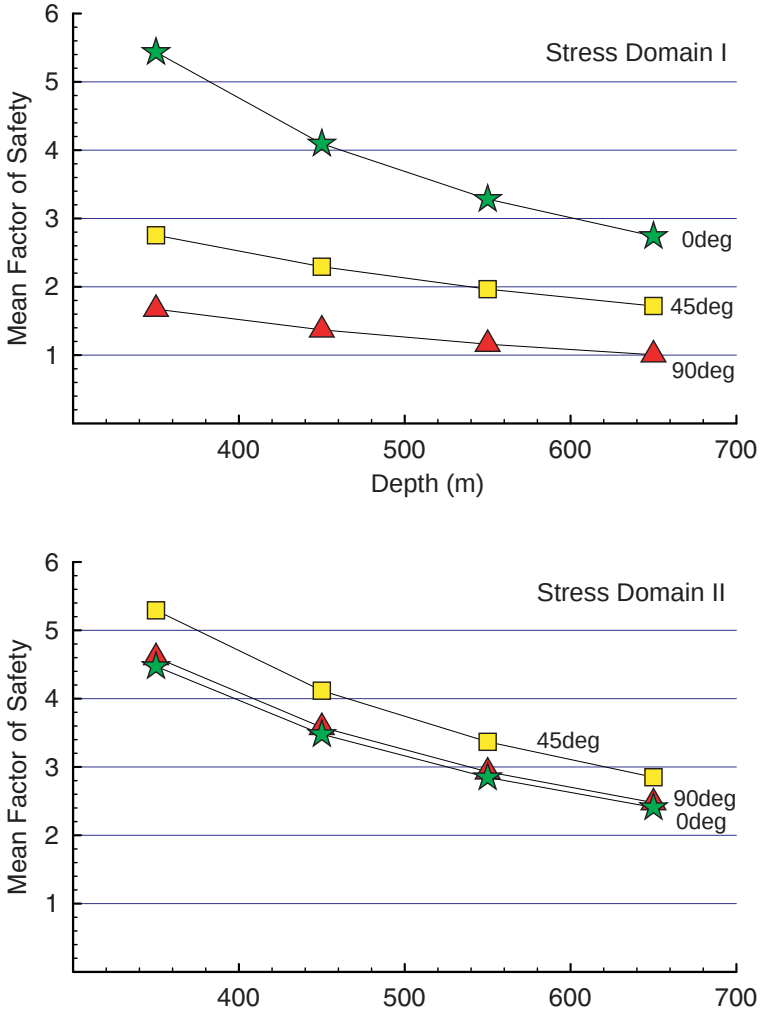

Figure 6–4: *Laxemar: Spalling instability for deposition tunnels in Stress Domains I and II.*

will likely encounter minor spalling below 500 m depth (Figure 6–5). The anticipated depth of spalling is given in Figure 6–6.

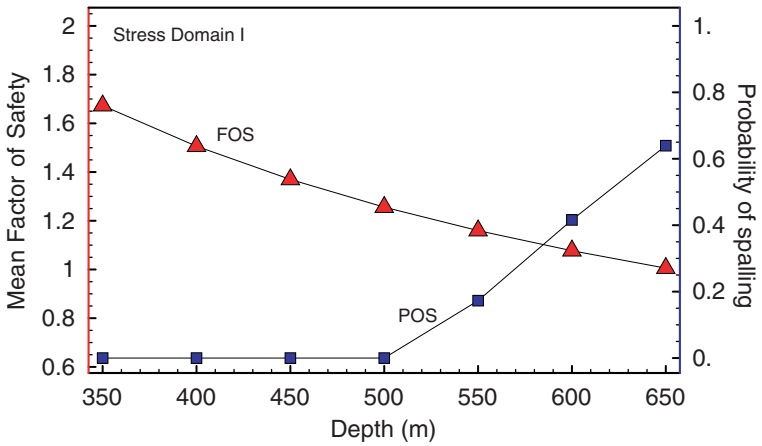

Figure 6–5: *Laxemar: Probability of spalling for deposition tunnels oriented perpendicular to the maximum horizontal stress in Stress Domain I.*

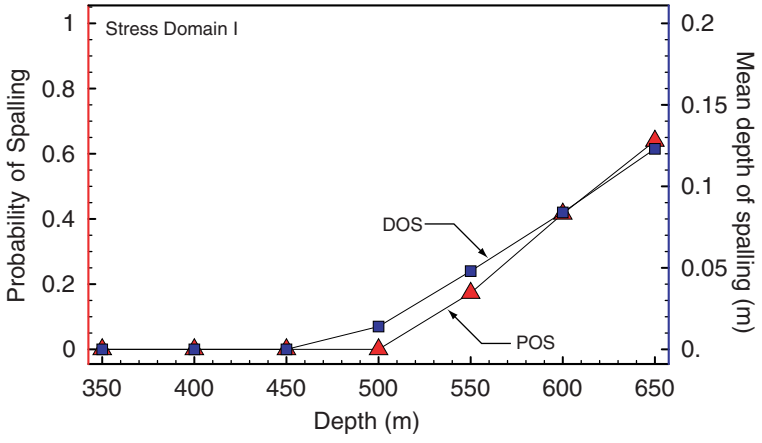

Figure 6–6: *Laxemar: Probability of spalling for deposition tunnels oriented perpendicular to the maximum horizontal stress in Stress Domain I and the corresponding mean depth of spalling.*

7 Conclusions

Underground excavations in a fractured sparsely rock mass may develop stability issues related to gravity induced falls-of-ground (wedges). The discrete fracture network for Forsmark has identified several joint sets. These joint sets were used in the underground wedge stability analysis program UnWedge. The results from these stability analysis indicated that any potentially unstable wedges would be adequately handled by standard rock bolt support systems. Hence, based on the current DFN model, there is no reason to base the depth of a repository or the orientation of the repository tunnels or caverns on wedge stability analyses. This notion is also supported by the construction experience from the Äspö Hard Rock Laboratory to depths of 450 m. This conclusion may need to be re-evaluated as the DFN model is refined and new information is added during the course of site investigation.

The results from SKB's in-situ Äspö Pillar Stability Experiment in a fractured crystalline rock mass supports the findings from AECL's Mine-by Experiment in a massive granitic rock mass and indicates that the rock mass spalling strength for crystalline rocks can be estimated as 0.57 ± 0.02 of the mean laboratory uniaxial compressive strength. This value is only slightly above the onset of crack initiation (dilation) measured in laboratory samples. A probability-based methodology utilizing this in-situ rock mass spalling strength has been developed for assessing the potential for spalling for Forsmark, Simpevarp and Laxemar sites. This methodology was calibrated against the underground experience at Äspö and AECL's Underground Research Laboratory. The in-situ stresses and the laboratory uniaxial compressive strength data from the Forsmark, Simpevarp and Laxemar sites were used as the bases for the analyses.

It should be noted that the confidence in the results from these analyses is directly related to the confidence in the input data. The greatest uncertainty in the input parameters is related to the in-situ stress magnitudes and the variation of these magnitudes with depth. This uncertainty will be reduced as the Site Description Models are improved.

Findings from the analyses to evaluate the potential for spalling indicates the following:

Forsmark site

1. At a repository depth of 650 m the probability for spalling in the vertical deposition holes increase to 10%.
2. The risk for spalling in the deposition tunnels oriented perpendicular to the maximum horizontal stress increases significantly below a repository depth of 450 m. This risk is eliminated at all repository depths if the deposition tunnels are oriented parallel to the maximum horizontal stress.
3. A central area of the repository will utilize a series of caverns/rooms with varying cross sections. These caverns should be oriented parallel to the maximum horizontal stress to minimize the risk for spalling

Simpevarp Site

1. Two stress domains have been identified for the Simpevarp site. In stress

domain II, there is no potential for spalling in either the vertical deposition boreholes or the deposition tunnels, regardless of tunnel orientation relative to the maximum horizontal stress.

2. Stress Domain I: The risk for spalling in the vertical deposition holes increases below a repository depth of 450 m. At 550 m depth the probability of spalling is approximately 20% while at a repository depth of 650 m the probability for spalling increases to approximately 70%.

3. Stress Domain I: The analyses indicate that the probability for spalling in deposition tunnels at a depth of 650 m is greater than 50% when those tunnels are oriented perpendicular to the maximum horizontal stress. At a depth of 550 m the probability of spalling for these tunnels is reduce to approximately 10%. The risk for spalling is eliminated if the deposition tunnels are oriented either parallel or at up to 45 degrees to the maximum horizontal stress, regardless of the repository depth.

Laxemar Site

1. Two stress domains have been identified for the Laxemar site. In stress domain II, there is no potential for spalling in either the vertical deposition boreholes or the deposition tunnels, regardless of tunnel orientation relative to the maximum horizontal stress.

2. Stress Domain I: The risk for spalling in the vertical deposition holes increases below a repository depth of 500 m. At 550 m depth the probability of spalling is approximately 20% while at a repository depth of 650 m the probability for spalling increases to approximately 60%.

3. Stress Domain I: The analyses indicate that the probability for spalling in deposition tunnels at a depth of 650 m is greater than 50% when those tunnels are oriented perpendicular to the maximum horizontal stress. At a depth of 550 m the probability of spalling for these tunnels is reduce to approximately 5 %. The risk for spalling is eliminated if the deposition tunnels are oriented either parallel or at up to 45 degrees to the maximum horizontal stress, regardless of the repository depth.

General Oskarshamn Region

The in-situ stress magnitudes measured at the Äspö Hard Rock Laboratory (HRL) appear to be similar in magnitudes to the in-situ stress magnitudes measured in Stress Domain I at Simpevarp and Laxemar. The rock mass quality and strength also appear to be similar at all sites in the Oskarshamn region. Tunnels and caverns of various profiles were excavated as part of the construction of the Äspö HRL. These openings have remained stable since being excavated in the mid-1990s. Spalling has not been observed in any of the Äspö HRL excavations except the Pillar Stability Experiment, where it was purposely created. There are no reasons to suspect that underground excavations in the Simpevarp and Laxemar area would perform any differently from the performance of the excavations at the Äspö HRL down to a depth of at least 450 m. An evaluation of the Äspö Prototype Repository (depth 450 m) deposition holes gave a factor of safety against spalling of approximately 1.5.

References

Andersson C, **2005**. Äspö pillar stability experiment. In *Bergmeckanikdag,* Stockholm (Ed. **Franzén T**), pp. 69–78, SveBeFo, Stockholm.

Andersson, C, Martin, CD, **2003**. Stress variability and the design of the Äspö Pillar Stability Experiment. In *Proc. 3rd Int. Symp. on Rock Stress,* Kumamoto, Eds. Sugawara, K, Obara, Y, Sato, A,pp. 321–326, A.A. Balkema, Rotterdam.

Andersson C, Martin CD, Christiansson R, **2004**. SKB s Äspö Pillar Stability Experiment, Sweden. In *CD-ROM Proc. 6th North American Rock Mechanics Symposium - NARMS04,* Houston (Eds. Yale DP, Willson SM, Abou-Sayed AS), pp. 1–8, NARMS 04-503.

Barton CA, Zoback MD, L BK, **1988**. *In situ* stress orientation and magnitude at the Fenton geothermal site, New Mexico, determined from wellbore breakouts. *Geophysical Research Letters*, 15(5):467–470.

Brace WF, Paulding B, Scholz C, **1966**. Dilatancy in the fracture of crystalline rocks. *Journal Geophysical Research*, 71:3939–3953.

Brudy M, Zoback MD, Fuchs K, Rummel F, Baumgärtner, **1995**. Estimation of the comlpete stress tensor to 8 km depth in the KTB scientific drill holes: Implications for crustal strength. *Journal Geophysical Research*, 102(B8):18453 – 18475.

Canadian Standard Association, **1991**. Risk analysis requirements and guidelines. Tech. Rep. CAN/CSA-Q634-91, Quality Management-A National Standard of Canada, Rexdale (Toronto), Canada, 42p.

Carlsson A, Christiansson R, **1986**. Rock stress and geological structures in the Forsmark area. In *Proc. Int. Symp. on Rock Stressand Rock Stress Measurements,* Stockholm (Ed. Stephansson O), Centek Publishers, Lulea.

Hajiabdolmajid V, Kaiser PK, Martin CD, **2002**. Modelling brittle rock failure. *International Journal Rock Mechanics And Mining Science*, 39(6):731–742.

Hajiabdolmajid V, Kaiser PK, Martin CD, **2003**. Mobilised strength components in brittle failure of rock. *Géotechnique*, 53(3):327–336.

Hallbauer DK, Wagner H, Cook NGW, **1973**. Some observations concerning the microscopic and mechanical behaviour of quartzite specimens in stiff, triaxial compression tests. *International Journal Rock Mechanics Mining Science & Geomechanics Abstracts*, 10:713–726.

Lindfors U, Perman F, Sjöberg, **2005**. Forsmark site investigation: Evaluation of the overcoring results from borehole KFM01B. Project P-05-66, Swedish Nuclear Fuel and Waste Management Company, Stockholm.

Martin CD, **1997**. Seventeenth Canadian Geotechnical Colloquium: The effect of cohesion loss and stress path on brittle rock strength. *Canadian Geotechnical Journal*, 34(5):698–725.

Martin CD, Chandler NA, **1994**. The progressive fracture of Lac du Bonnet granite. *International Journal Rock Mechanics Mining Science & Geomechanics Abstracts*, 31(6):643–659.

Martin CD, Christainsson R, Söderhäll J, **2001**. Rock stability considerations for siting and constrcuting a KBS3 repository: Based on experiences from Äspö HRL, AECL's URL, tunnelling and mining. Technical Report TR-01-38, Swedish Nuclear Fuel and Waste Management Company, Stockholm.

Martin CD, Christiansson R, **1991**. Overcoring in highly stressed granite – The influence of microcracking. *International Journal Rock Mechanics Mining Science & Geomechanics Abstracts*, 28(1):53–70.

Martin CD, Kaiser PK, McCreath DR, **1999**. Hoek-Brown parameters for predicting the depth of brittle failure around tunnels. *Canadian Geotechnical Journal*, 36(1):136–151.

Martin CD, Read RS, **1996**. AECL's Mine-by Experiment: A test tunnel in brittle rock. In *Proc. 2nd North American Rock Mechanics Symposium*, Montreal (Eds. Aubertin M, Hassani F, Mitri H), vol. 1, pp. 13–24, A.A. Balkema, Rotterdam.

Martin CD, Read RS, Martino JB, **1997**. Observations of brittle failure around a circular test tunnel. *International Journal Rock Mechanics And Mining Science*, 34(7):1065–1073.

Martin CD, Stimpson B, **1994**. The effect of sample disturbance on laboratory properties of Lac du Bonnet granite. *Canadian Geotechnical Journal*, 31(5):692–702.

Morgenstern N, **1995**. The 3rd Casagrande Lecture: Managing risk in geotechnical engineering. In *Proc. 10th Pan-American Conference on Soil Mechanics and Foundation Engineering*, Guadalajara, Mexico, vol. 4, p. 102 126, Mexican Society of Soil Mechanics, Mexico City.

Peng SS, Johnson AM, **1972**. Crack growth and faulting in cylindrical specimens of Chelmsford granite. *International Journal Rock Mechanics Mining Science & Geomechanics Abstracts*, 9:37–86.

Potyondy DO, Cundall PA, **2004**. A bonded-particle model for rock. *International Journal Rock Mechanics And Mining Science*, 41(8):1329–1364.

Read RS, **1994**. *Interpreting excavation-induced displacements around a tunnel in highly stressed granite*. Ph.D. thesis, Department of Civil & Geological Engineering, University of Manitoba, Winnipeg, Manitoba, Canada.

Read RS, Martino JB, Dzik EJ, Chandler NA, **1997**. Excavation stability study – Analysis and interpretation of results. OPG 06819-REP-01200-0028-R00, Ontarion Hydro, Nuclear Waste Management Division, Toronto.

Scholz CH, **1968**. Microfracturing and the inelastic deformation of rock in compression. *Journal Geophysical Research*, 73(4):1417–1432.

Sjöberg J, **2004**. Forsmark site investigation: Overcoring rock stress measurements in borehole KFM01B. Tech. Rep. SKB P-04-83, Swedish Nuclear Fuel and Waste Management Company, Stockholm, Sweden.

SKB, **2004**. Deep repository. Underground design premises. Edition d1/1. R-report R-04-60, Svensk kärnbränslehantering AB, Stockholm.

SKB, **2005**a. Forsmark Site Description Model v1.2. R-report R-05-18, Svensk kärnbränslehantering AB, Stockholm.

SKB, **2005**b. Simpevarp Site Description Model v1.2. R-report R-05-08, Svensk kärnbränslehantering AB, Stockholm.

Stacey TR, **1981**. A simple extension strain criterion for fracture of brittle rock. *International Journal Rock Mechanics Mining Science & Geomechanics Abstracts*, 18:469–474.

Stille H, Andersson J, Olsson L, **2003**. Information based design in rock engineering. SveBeFo Rapport 61, SveBeFo, Swedish Rock Engineering Research, Stockholm, Sweden, 147p.

Appendices

A Rock mass spalling strength

A.1 Background

Failure of underground openings in hard rocks is a function of the in-situ stress magnitudes and the characteristics of the rock mass, i.e., the intact rock strength and the fracture network. At low in-situ stress magnitudes, the failure process is controlled by the continuity and distribution of the natural fractures in the rock mass. However as in-situ stress magnitudes increase, the failure process is dominated by new stress-induced fractures growing parallel to the excavation boundary. This fracturing is generally referred to as spalling failure or extension fracturing. Initially, at intermediate depths, these stress-induced spalling regions are localized near the tunnel perimeter and tend to form v-shaped notches (Figure A.1).

Martin et al. /1997/ described the brittle-failure process observed around AECL's Mine-by test tunnel. The test tunnel was extensively instrumented and Martin /1997/ showed that the onset of spalling was related to the onset of cracking in the rock mass as recorded by a microseismic monitoring array. Their results clearly showed that the onset of cracking in-situ commenced well before the peak strength recorded in uniaxial compressive tests. Several researchers, e.g. /Brace et al. 1966; Scholz 1968; Peng and Johnson 1972; Hallbauer et al. 1973; Martin and Chandler 1994/, have shown that the onset of dilation in brittle rocks is represented by the initiation of extension fracturing (crack initiation) in uniaxial laboratory compression tests and that these extension fractures also initiate well before the peak strength is reached as illustrated in Figure A.2. Laboratory tests by these researchers have shown that the onset of dilation (Crack Initiation) typically occurs between 0.4 and 0.6 of the peak strength for a wide variety of rock types and concrete.

Stacey /1981/ using elastic analyses introduced the concept of extensional strain to estimate the extent of spalling around South African underground mines. Stacey /1981/ determined the extensional strain from laboratory compression tests using plots of lateral

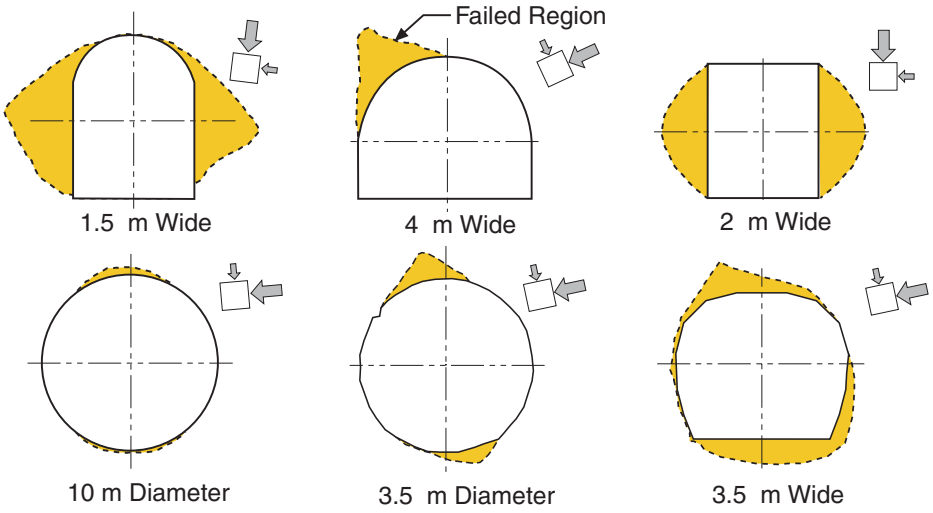

Figure A.1: *Extent and shape of stress-induced spalling failure observed around various shaped underground openings, after Martin et al. /1999/.*

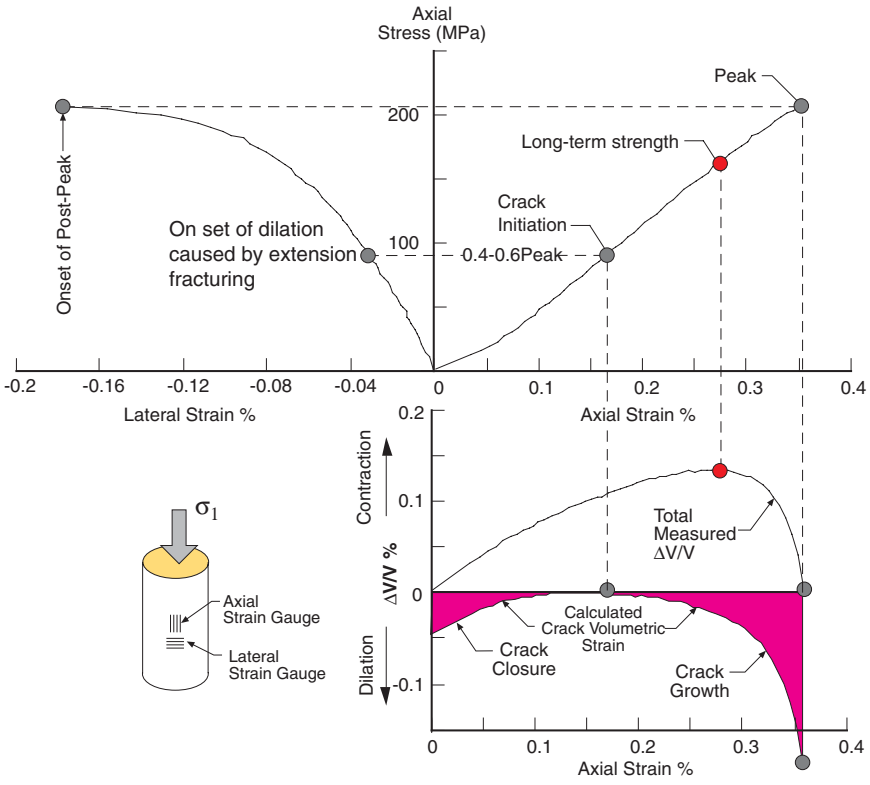

Figure A.2: *Stress-strain curves for Lac du Bonnet granite, data from Martin and Chandler /1994/. Note that the onset of dilation occurs at approximately 50% of the peak uniaxial strength.*

strain versus axial strain. Stacey /1981/ defined the the critical extension strain as the lateral strain at the onset of nonlinearity in the lateral strain versus axial strain plot. It can be seen in Figure A.2 that if one makes such a plot the critical extensional strain defined by Stacey /1981/ is identical to the onset of dilation. Martin /1997/ used the same concept, expressed in terms of crack initiation[10] to evaluate the depth of spalling around the Mine-by Test tunnel. Martin et al. /1999/ applied this logic to develop the depth of spalling-failure given by:

$$\frac{D_f}{a} = 0.48 + 0.5\frac{\sigma_{\theta\theta}}{\sigma_{sm}} \qquad \text{(A.1)}$$

The depth of spalling given by Equation A.1 is an empirical criterion restricted to approximately circular excavations. For non-circular excavations or when more detailed information is required the depth of spalling can be determined using a numerical analysis and a spalling failure criterion. Because the spalling process occurs via extension fracturing, the cohesive strength component dominates the peak-failure envelope while the frictional component can be ignored. However, once spalling has occurred the cohesive strength component of the residual-failure envelope is significantly reduced while the frictional component is fully mobilized. Figure A.3 shows the spalling-failure envelope used to predict the depth of spalling for the Mine-by test tunnel compared to the measured depth of spalling. Once the depth of spalling has been assessed using this approach, the support can be determined assuming that the entire weight of the spalled region must be retained by the support system. Alternatively, if no support will be used this method can be

[10] At the time of the development of Equation 3, Crack initiation was considered a lower bound estimate and approximately equal to the rock mass spalling strength

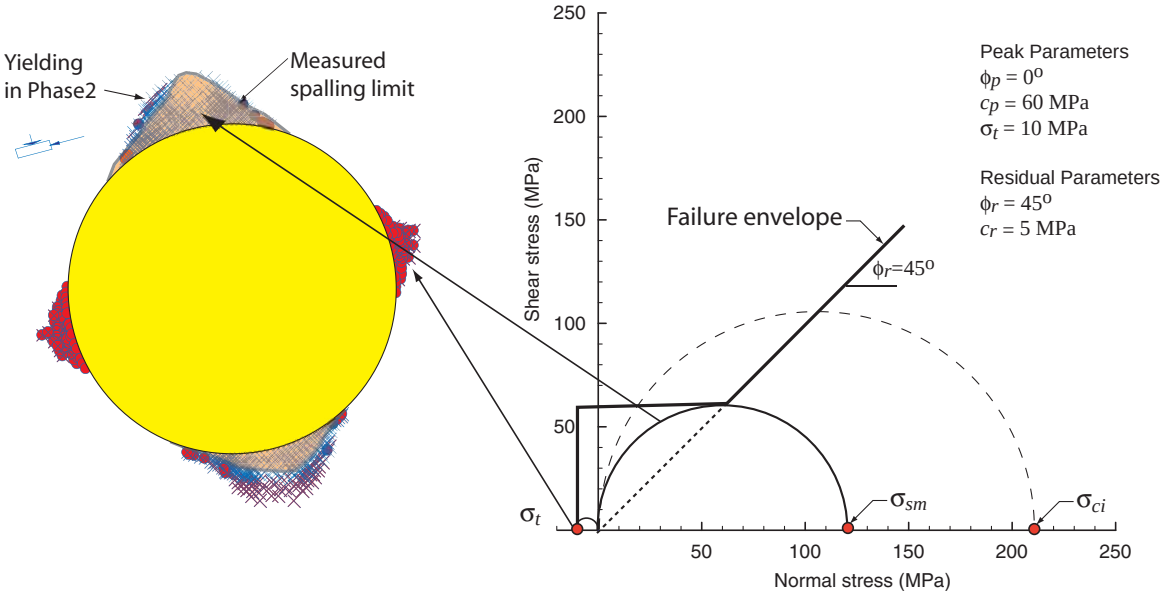

Figure A.3: *Predicted brittle failure around the Mine-by test tunnel compared with the observed failure. The predicted failure used Phase2 and a spalling failure criterion.*

used to estimate the depth of the v-shaped notch that will develop.

Since the mid-1990's with the development of the discrete element numerical codes (such as Particle Flow Code) researchers can now numerically replicate the stress-strain curve in Figure A.2 numerically Potyondy and Cundall /2004/. This ability has provided additional insight into the behaviour of brittle rocks in compression and supports the spalling-failure envelope discussed above. In particular, it has shown that the onset of dilation (crack initiation) is controlled more by the geometry of the grains than the material properties. This helps to explain why the onset of dilation in rocks where the grain size is small and relatively uniform, typically occurs near the peak strength rather than at the 0.4 to 0.6 observed in medium to coarse grained crystalline rocks.

A.2 Rock mass spalling strength from in-situ experiments

Two in-situ have experiments have been carried out to investigate brittle failure, i.e., spalling: AECL's Mine by Experiment and SKB's ASPO Pillar Stability Experiment.

A.2.1 AECL's Mine-by Experiment

The first phase of AECL's Mine-by Experiment, the excavation of a 3.5-m-diameter tunnel, was carried out at the 420 Level of AECL's Underground Research Laboratory from 1990 to 1995 to investigate progressive failure around a circular opening in brittle, unfractured Lac du Bonnet granite (Figure A.4). The tunnel was excavated without explosives, and state-of-the-art instrumentation comprising both geomechanical and geophysical instruments was used to monitor the failure process. The in-situ experiment was supplemented by extensive laboratory tests. The major conclusion from the Mine-by Experiment was that spalling initiated when the maximum tangential stress on the boundary of the tunnel reached 120 MPa. The mean uniaxial compressive strength of Lac du Bonnet granite was given as 212 MPa, therefore the onset of spalling could be

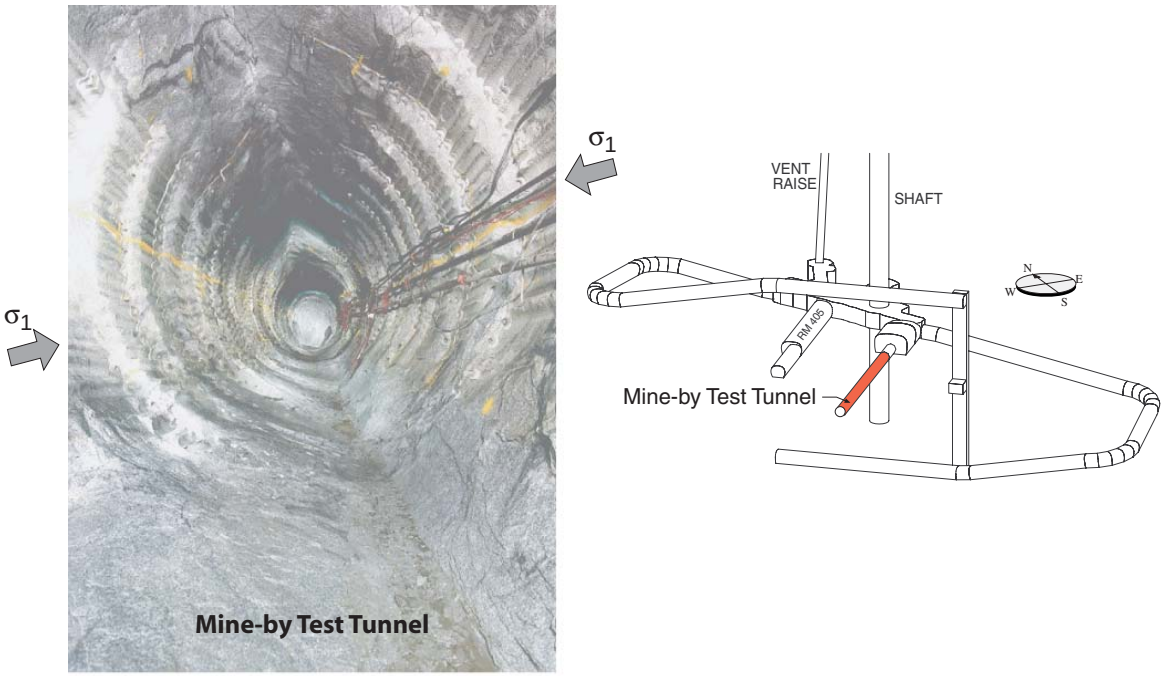

Figure A.4: *Layout of the Mine-by Experiment and a photo of the excavated test tunnel.*

expressed as $120/212 = 0.56$UCSm.

This 120 MPa value was also confirmed by Read et al. /1997/ by excavating tunnels with various shapes and various orientations relative to the in-situ stress state at the 450 Level. Their work concluded there was little variation in the tangential stress required to initiate spalling in the medium-grained granite suggesting that the local variation in the granite rock mass strength and in-situ stress magnitudes was minor. However, Read et al. /1997/ noted that the tangential stress required to initiate spalling in the fine grained granodiorite was approximately 150 MPa, despite the granoditoite only having a modest increase in the uniaxial compressive strength. Only a few observations were made at the URL, but it was clear that the grain size of the rock had a significant effect on the stress magnitude required to initiate spalling.

A.2.2 Äspö Pillar Stability Experiment

The Äspö Pillar Stability Experiment (APSE) is in progress and only preliminary results are reported here. The APSE was excavated at the 420-m depth of Äspö Hard Rock Laboratory and examined spalling in a fractured rock mass and thermo-mechanical coupling (Figure A.5). The excavation of two 1.8-m-diameter boreholes, separated by 1-m-thick pillar, was purposely over-stressed, using excavation- and thermally-induced stresses, to induce spalling in the pillar Andersson et al. /2004/ (Figure A.6). The stresses in the pillar were controlled and the onset of spalling monitored using acoustic emission instrumentation and deformations. The major difference between the APSE and the Mine-by Experiment is that APSE was located in fractured rock but the intact uniaxial strength of Aspo Diorite is similar to that of Lac Du Bonnet Granite, i.e., 210 and 212 MPa, respectively.

Table A.1 compares the rock mass spalling strength determined from APSE and the

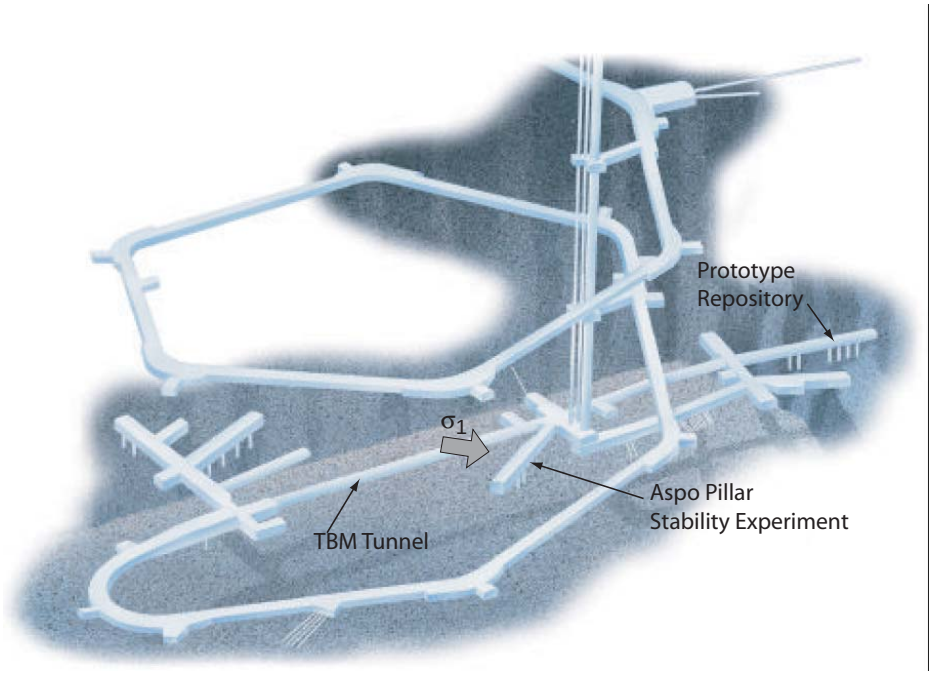

Figure A.5: *Location of the Äspö Pillar Stability Experiment and the Prototype Repository.*

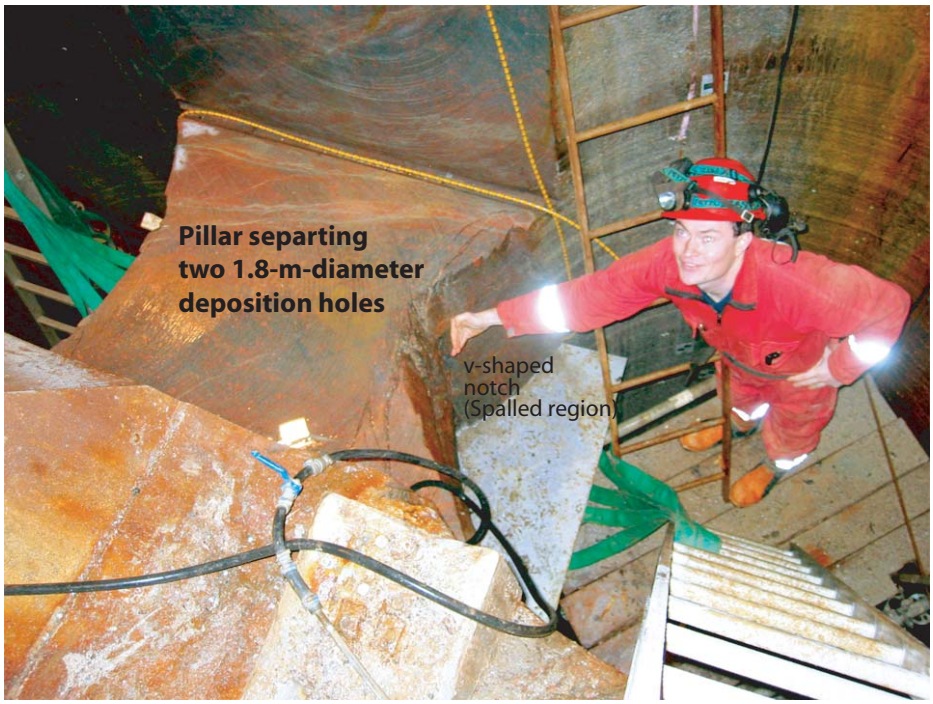

Figure A.6: *Photograph of the Äspö Pillar Stability Experiment, showing the extent of the notch in the 1-m-thick pillar.*

Mine-by Experiment. This data was then used with the methodology described in Figure 3–7 to evaluate the approach.

Table A.1: Summary of the on set of dilation (crack initiation) measured in laboratory tests and the rock mass spalling strength from in-situ tests. The mean peak uniaxial compressive strength (UCSm) is used as the reference strength.

Underground Facility	Laboratory Mean Values			In-situ Spalling Strength	
	CI (MPa)	CI/UCS	UCSm (MPa)	σ_{sm} (MPa)	σ_{sm}/UCSm
Äspö Pillar Stability Experiment					
Aspo Diorite	94	0.44	211	119 ± 6	0.56 ± 0.03
Mine-by Experiment					
Lac du Bonnet granite	97	0.45	212	120	0.56
Granodiorite	120	0.52	228	150	0.65

B Forsmark Uniaxial Compressive Strength

Table B.1: Summary of the test results from uniaxial uncon• ned compression tests for Forsmark. The peak strength is given as the uniaxial compressive strength (UCS).

Specimen ID	Borehole Depth (m)	ACTUAL DEPTH (m)	Density (kg/m^3)	Crack Initation (CI) MPA	CI / UCS	Long-term Strength (MPa)	UCS (MPa)	Young's modulus (GPa)	Poisson's ratio
KFM04A-113-1	162.02	140.41	2670	130	0.52	233	249.1	76.56	0.24
KFM04A-113-3	162.62	140.93	2690	130	0.54	208	241.1	80.68	0.25
KFM04A-113-5	163.51	141.70	2680	112	0.50	200	221.8	78.22	0.19
KFM04A-113-6	163.65	141.82	2700	116	0.50	190	230.1	73.44	0.23
KFM01A-113-1	225.92	224.96	2660	142	0.53	244	270.1	81.90	0.24
KFM01A-113-2	226.09	225.13	2660	187	0.69	243	269.7	78.15	0.21
KFM01A-113-3	227.23	226.27	2650	182	0.83	220	220.4	79.09	0.25
KFM01A-113-4	228.00	227.03	2660	100	0.45	210	224.1	74.05	0.22
KFM01A-113-5	229.60	228.63	2650	128	0.56	215	227.0	79.79	0.28
KFM02A-113-1	333.51	332.42	2660	120	0.54	195	221.3	78.56	0.24
KFM02A-113-2	333.66	332.57	2660	115	0.52	200	221.5	76.06	0.22
KFM02A-113-3	334.11	333.02	2660	-	-	195	226.9	74.13	0.16
KFM02A-113-4	334.52	333.43	2660	115	0.53	192	218.1	73.53	0.26
KFM02A-113-5	334.78	333.69	2660	112	0.54	185	209.2	75.28	0.21
F01A-113-13	495.61	493.51	2662	130	0.54		239.2	74.20	0.29
KFM01A-113-8	496.01	493.91	2660	102	0.54	165	187.4	78.91	0.24
F01A-113-9	496.3	494.19	2660	120	0.51		234.3	75.00	0.29
KFM01A-113-10	496.45	494.34	2650	120	0.52	201	229.3	76.11	0.20
F01A-113-11	496.74	494.63	2642	125	0.51		247.3	75.90	0.29
KFM01A-113-12	496.74	494.63	2660	160	0.61	229	261.6	76.47	0.22
KFM01A-113-14	497.14	495.03	2660	101	0.42	229	238.9	74.23	0.18
F01A-113-15	497.42	495.31	2664	125	0.53		236.9	75.80	0.30
KFM01A-113-16	497.42	495.31	2660	126	0.53	204	235.6	75.31	0.23
F01A-113-17	497.71	495.60	2656	128	0.54		237.0	75.00	0.28
KFM01A-113-18	497.76	495.65	2660	125	0.43	220	288.6	78.00	0.18
F01A-113-19	498.04	495.93	2661	126	0.53		237.7	75.20	0.30
KFM04A-113-7	586.46	508.24	2650	110	0.51	176	217.8	73.02	0.24
KFM04A-113-8	586.60	508.37	2650	123	0.51	188	238.9	74.90	0.29
KFM04A-113-9	586.73	508.48	2650	133	0.54	200	244.9	75.00	0.26
KFM04A-113-10	586.95	508.67	2660	120	0.54	182	221.0	77.26	0.26
KFM04A-113-11	587.42	509.07	2660	113	0.51	172	221.3	75.11	0.28
KFM03A-113-15	523.82	522.37	2650	123	0.54	190	227.8	76.28	0.27
KFM03A-113-16	523.96	522.51	2650	120	0.57	180	209.1	71.36	0.25
KFM03A-113-17	524.09	522.64	2660	105	0.52	168	203.5	73.43	0.21
KFM03A-113-18	524.87	523.42	2650	124	0.57	190	217.4	77.74	0.25
KFM02A-113-7	527.72	526.00	2650	110	0.50	210	219.5	77.18	0.23
KFM02A-113-8	528.00	526.28	2650	92	0.48	175	193.3	78.60	0.20
KFM02A-113-9	528.91	527.18	2650	85	0.51	133	166.4	76.62	0.24
KFM02A-113-10	529.33	527.60	2660	134	0.55	215	241.7	77.42	0.21
KFM03A-113-22	670.54	668.69	2660	110	0.54	177	202.6	70.61	0.24
KFM03A-113-23	670.68	668.83	2660	120	0.48	200	251.1	72.81	0.22
KFM03A-113-24	670.82	668.97	2660	122	0.54	195	226.2	77.08	0.23
KFM03A-113-25	671.08	669.23	2650	128	0.56	190	227.2	80.10	0.25
KFM01A-113-20	690.32	687.39	2660	120	0.53	203	224.6	77.83	0.27
KFM01A-113-21	690.46	687.53	2650	130	0.52	219	248.0	76.51	0.23
KFM01A-113-22	690.60	687.67	2660	108	0.51	200	213.3	76.13	0.14
KFM01A-113-23	690.74	687.81	2650	120	0.48	223	249.1	77.86	0.24
KFM02A-113-13	705.55	703.25	2650	117	0.53	192	222.0	77.00	0.25
KFM02A-113-14	705.70	703.40	2660	107	0.53	186	202.0	73.27	0.20
KFM02A-113-15	705.85	703.55	2650	102	0.46	200	220.5	71.67	0.18
KFM04A-113-13	812.78	704.39	2660	114	0.55	170	207.8	72.93	0.28
KFM04A-113-14	812.92	704.51	2660	105	0.53	170	199.2	73.48	0.25
KFM04A-113-15	813.06	704.63	2660	100	0.49	175	205.4	72.09	0.25
KFM04A-113-16	813.20	704.75	2660	95	0.49	160	192.1	69.45	0.23
KFM04A-113-17	813.64	705.13	2660	95	0.52	174	183.1	71.29	0.21
KFM02A-113-16	708.25	705.94	2650	112	0.53	191	209.4	77.24	0.26
KFM02A-113-17	708.40	706.09	2650	113	0.53	187	213.6	75.28	0.22

C Simpevarp Uniaxial Compressive Strength

Table C.1: Summary of the test results from uncon• ned compression tests for Simpevarp.

Borehole	BH Depth (m)	Wet Density (kg/m**3)	Dilation (MPa)	UCS (MPa)	Young 50 (GPa)	Poissons Ratio 50
KSH01A	299.27	2770	79.0	158.3	70.7	0.31
KSH01A	301.66	2770	80.0	167.7	68.5	0.33
KSH01A	303.04	2780	65.0	170.4	69.0	0.28
KSH01A	311.21	2790	92.0	192.9	86.1	0.32
KSH01A	319.59	2810	95.0	186.0	80.7	0.33
KSH01A	401.48	2780	95.0	246.8	84.0	0.25
KSH01A	413.16	2780	48.0	109.3	81.5	0.24
KSH01A	486.05	2810	89.0	181.6	77.6	0.31
KSH01A	491.95	2800	62.0	142.1	80.5	0.26
KSH01A	494.81	2790	110.0	229.5	78.6	0.28
KSH01A	495.57	2790	90.0	171.5	100.5	0.27
KSH01A	699.67	2830	52.0	141.6	86.4	0.22
KSH01A	700.35	2830	65.0	133.1	77.0	0.27
KSH01A	702.38	2840	77.0	177.6	83.3	0.25
KSH01A	703.00	2830	87.0	160.2	82.6	0.24
KSH01A	703.15	2830	54.0	118.3	80.5	0.19
KSH02A	313.19	2790	194.0	244.4	85.4	0.26
KSH02A	313.33	2790	35.0	235.4	85.1	0.21
KSH02A	313.47	2790	95.0	263.8	90.9	0.27
KSH02A	323.23	2780	125.0	229.6	81.0	0.22

D Reliability of traditional in-situ stress measurements in high stress environment

D.1 Experience from 420 Level of AECL's URL

Once the sampling depth encounters in-situ stress magnitudes that are sufficient to start inducing microcrack damage in the core samples, the properties of these damaged samples no longer reflects the in-situ properties. Martin and Stimpson /1994/ clearly showed the effect of stress-induced sample disturbance on the properties of Lac du Bonnet granite. In-situ stress test results that rely on the interpretation of strains based on linear elastic theory also become suspect when stress-induced damage is encountered Martin and Christiansson /1991/.

Prior to the execution of AECL's Mine-by Experiment a series of overcore measurements were carried out using AECL's Modified CSIR Triaxial Strain cell at the 420 Level of AECL's URL. The results, based on the classical linear elastic solution, are shown as histograms in Figure D.1 and it is clear there was a large range in the stress magnitudes measured. At the end of the Mine-by Experiment, the in-situ stress tensor was back calculated using a variety of techniques based on large-scale displacement measurements Read /1994/. Martin and Read /1996/ gave the likely range in this back-calculated stress tensor magnitude as that shown in Figure D.1. It is clear from Figure D.1 that the back-calculated stress magnitudes for Sigma 1 and Sigma 2 were greater than the stress magnitudes given by the overcore test results.

This example is perhaps extreme as core discing was observed in nearly all the overcore samples and it was obvious that the linear elastic theory was not appropriate for the interpretation of the measure strains. However, despite the error the overcore results did provide stress magnitudes that were adequate for the preliminary design of development of the 420 Level, and the execution of the Mine-by Experiment. The important lesson, is that the over core results were indicating that the stress magnitudes were elevated, and that the measured stress magnitudes turned out to be lower bound stress magnitudes.

D.2 Forsmark stress data

In-situ stress data for this report were taken from Sjöberg /2004/. The magnitudes and orientations were determined in borehole KFM01B at a depth between 238-242 m (Level 1) using the Borre probe triaxial strain cell Lindfors et al. /2005/. Three successful tests were completed.

The average magnitude of σ_1 for Level 1 was reported as approximately 40 MPa. Below the Level 1 depth, overcoring encountered core-discing during the overcoring process. The author's experience suggests that if core discing is present the overcore data were immediately suspect because the linear elastic theory used to interpret the measured strains has been violated. It is also the author's experience that the overcore results, when core discing is present, show unrealistic scatter in magnitude and orientation. Hence, for the purposes of this report only the Level 1 triaxial data were used to establish the statistical variation at a given Level.

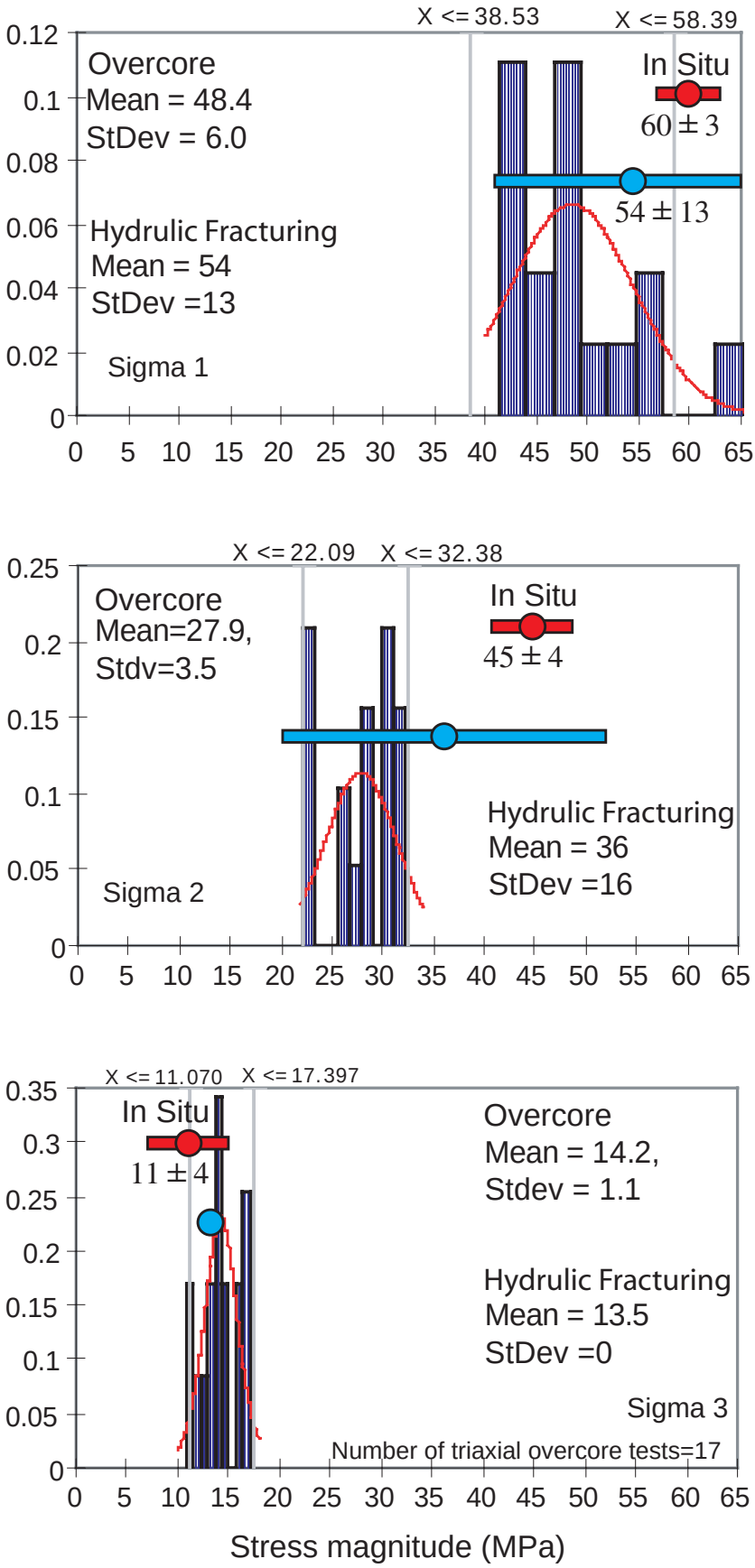

Figure D.1: *Comparison of the magnitudes from 17 triaxial overcore tests using AECL's Modified CSIR triaxial strain cell, with the back calculated in-situ stress magnitudes at the end of the Mine-by Experiment.*

The confidence interval for the Level 1 was established using the Excel macros provided by SKB Lindfors et al. /2005/. The results are given in Figure D.2. It was assumed that the range in the principal and horizontal stress magnitudes, determined from Level 1, was similar at all depths.

KFM01B - Level 1 - Hole Depth between 238-242 m:

Meas. No.	σ_1	Dip	Bearing	σ_2	Dip	Bearing	σ_3	Dip	Bearing
1	41.3	6.0	104.0	21.9	34.0	198.0	6.9	55.0	6.0
2	38.7	12.0	282.0	22.3	19.0	187.0	15.6	67.0	43.0
3	40.2	12.0	289.0	32.4	17.0	195.0	19.0	69.0	53.0
Average	**39.5**	**4.6**	**284.0**	**25.4**	**25.4**	**191.8**	**14.6**	**64.1**	**23.5**

Confidence Intervals for Level 1 Principal stresses

	Principal stresses								
	σ_1 [MPa]	**Dip** [°]	**Bearing** [°]	σ_2 [MPa]	**Dip** [°]	**Bearing** [°]	σ_3 [MPa]	**Dip** [°]	**Bearing** [°]
Average:	39.5	4.6	284.0	25.4	25.4	191.8	14.6	64.1	23.5
95% lower	37.8	*)		14.6			0.5		
95% upper	45.0			38.0			24.4		
90% lower	38.0	*)		16.0			2.1		
90% upper	44.1			36.7			23.1		
80% lower	38.4	*)		17.6			3.9		
80% upper	43.2			35.0			21.5		
Measured values & deviation									
Max :	+1.8	+7.0	+6.0	+7.0	+8.4	+6.3	+4.4	+4.7	+28.4
Min :	-0.8	1.5	-180.0	-3.5	-7.9	-3.0	-7.7	-8.6	-18.5
Max [%] :	+5%			+28%			+30%		
Min [%] :	-2%			-14%			-53%		

Confidence Intervals for Level 1 Horizontal stresses

	Vertical and Horizontal components				
	σ_H [MPa]	**Bearing** [°]	σ_h [MPa]	**Bearing** [°]	σ_v [MPa]
Average:	39.3	105.2	23.4	15.2	16.8
95% lower	37.1	*)	11.5		5.1
95% upper	42.6		34.3		28.5
90% lower	37.4	*)	12.9		6.6
90% upper	42.2		32.9		27.1
80% lower	37.8	*)	14.6		8.2
80% upper	41.8		31.3		25.4
Measured values & deviation					
Max :	+1.7	+10.2	+7.7	+10.2	+4.3
Min :	-1.5	-3.0	-6.2	-3.0	-4.8
Max [%] :	+4%		+33%		+26%
Min [%] :	-4%		-26%		-29%

Figure D.2: *In-situ stress from KFM01B at Level 1 and the associated confidence intervals. Data from Martin et al. /2001/.*